POLITECNICO DI MILANO
School of Industrial and Information Engineering
Master of Science in Mechanical Engineering

CFD modeling of constant-volume Diesel combustion considering conventional and alternative fuels

Supervisor:
Prof. Tommaso LUCCHINI

Author:
Emre SANCAR
Matr. 872037

Academic Year 2017 – 2018

To our beloved families, friends and all the teachers who are volunteers of science

Acknowledgments

Firstly, I would like to express my sincere gratitude to Prof. Tommaso Lucchini for his support to my master studies and the motivation and impressive knowledge he has given to me. His guidance helped me in all the aspects of researching and implementing of this study in Politecnico di Milano, I could not have imagined having a better advisor for my master study.

Furthermore, I would like to thank to Prof. Gianluca D'Errico who provided me a chance to work with Politecnico di Milano Internal Combustion Engines Group.

I want to give special appreciations of mine to my parents and brother for their endorsement and encouragement during all my education life. This accomplishment would not have been possible without them.

Finally, my sincere thanks also go to my friends, especially who share the same experience with me in my Milano days, for their help and friendship. I am glad that I have them.

Content

List of Figures

List of Tables

Abstract

The aim of this thesis is to analyze non-premixed combustion which is also referred to diesel combustion with four different combustion models which are Representative Interactive Flamelet (RIF) Model, Tabulated Well-Mixed (TWM) Model, Tabulated Representative Interactive Flamelet (TRIF) Model and Approximated Diffusion Flamelet (ADF) Model. In addition to this, different chemistry mechanisms and fuels are validated with RIF model. Soot formation prediction is also one of the parts of this study by adapting semi-empirical soot model by Leung et al. into TWM model since tabulation gives benefit on time consideration.

CFD simulations are performed under constant volume vessel by using OpenFOAM which is a Linux based open source CFD tool. Lib-ICE application and libraries are developed by Politecnico di Milano Internal Combustion Engine Group and they are used to perform combustion simulations with described models since all solvers are already included in libraries. Validation of the simulations are exercised by experimental data provided by Sandia National Laboratories, Engine Combustion Network.

First of all, the behavior of combustion models is tested with n-dodecane fuel under different operating conditions with respect to experimental one in order to understand how models are capable of predicting combustion phenomena accurately in terms of heat release rate and maximum temperature within the vessel. After validation of the combustion models, trend for soot particle formation are exercised with TWM model by changing the particular constants defined in soot model and behavior of DME which is an alternative fuel for diesel engines is investigated with validated RIF combustion model.

Keywords: *CFD, Diesel Combustion, OpenFOAM, RIF, TRIF, TWM, ADF, Lib-ICE, DME*

Sommario

Lo scopo della presente tesi è quello di analizzare la combustione non premiscelata, tipica nei motori Diesel, attraverso l'utilizzo di quattro diversi modelli: Representative Interactive Flamelet (RIF), Tabulated Well-Mixed (TWM), Tabulated Representative Interactive Flamelet (TRIF) e Approximated Diffusion Flamelet (ADF). Inoltre, diversi meccanismi di cinetica chimica e combustibili sono testati, utilizzando il modello RIF. I modelli a cinetica tabulata riescono a dare rilevanti vantaggi in termini di costi computazionali: la formazione di soot è quindi esaminata grazie al utilizzo del modello semi-empirico proposto da Leung et al., applicato al modello di combustione TWM.

Le analisi CFD sono eseguite all'interno della camera di combustione a volume costante, utilizzando OpenFOAM, che è un applicazione open source implementata nel ambiente Linux. I solutori e le librerie della Lib-ICE sono stati sviluppati dal gruppo Internal Combustion Engine del Politecnico di Milano, questi sono stati utilizzati per eseguire le simulazioni di combustione con i modelli sopra citati. La validazione delle simulazioni è proposta utilizzando i dati sperimentali forniti da Sandia National Laboratories, Engine Combustion Network.

Innanzitutto, il comportamento dei modelli di combustione è testato con n-dodecane combustibile considerando diverse condizioni operative, con lo scopo di ottenere informazioni sulla capacità dei modelli di predire con accuratezza il fenomeno di combustione, in termini di heat release rate e massima temperatura all'interno del camera. Successivamente alla convalida, l'andamento della formazione delle particelle di soot è analizzata testando e tarando le costanti definite da Leung et al., il modello di combustione TWM è stato utilizzato. Infine il comportamento del DME, il quale è un combustibile alternativo per motori Diesel, è studiato con il modello di combustione RIF.

Parole chiavi: *CFD, Combustione Diesel, OpenFOAM, RIF, TRIF, TWM, ADF, Lib-ICE, DME*

Introduction

Internal combustion engines are one of the main machines to produce mechanical energy from fuel chemical energy. The term internal refers to a combustion process of fuel inside the cylinder. Internal combustion engines can be classified in two sub-categories which are spark-ignition (gasoline) and compression-ignition (diesel) engines. Nowadays, diesel engines are one of the most popular options in many areas such as transportation and energy production; furthermore, the reason for increasing demand for diesel engines can be explained by its high thermal efficiency and high power-weight ratio compared to other engines. However, pollutant emissions should be taken into consideration in addition to thermal efficiency of the machine since overall contribution from the engines is remarkable in terms of emission. Due to diffusive combustion nature of the diesel engine, soot formation problem comes to existence. Researches are made to improve combustion process of diesel engine by considering increase in efficiency and reduction in emissions and specific fuel consumption since emission legislation has strictly increased restriction demand especially in European Union. Improvement of the combustion phenomena can be obtained by synthesis of experimental and computational efforts. Modelling of combustion process provides significant advantage in terms of time and cost even though there are some uncertainties.

Computational Fluid Dynamics shortly CFD which solves several differential equations for mass, momentum and energy conservation, is a significant tool to predict and improve the combustion process by decreasing necessary time and cost. Moreover, it provides comparable results for engine parameters such as injection duration, compression ratio for development process. Computational Fluid Dynamics performs simulation by taking into account reacting flows and provides information for variable fields in addition to spatial distribution of chemical species. Besides, models which are accounted by CFD should be accurate also; thus, experimental validation is crucial to understand the accuracy of the combustion model for further development procedures.

Application of CFD for diesel combustion process which is very complex due to unsteady, turbulent and multi-phase nature of the combustion process is the

primary focus of this study. In earlier, combustion process is defined with heat release assuming infinitely fast chemical reactions; nevertheless, this approach is not sufficient to describe combustion phenomena like ignition, pollutant formation and transition from different phase of combustions. Therefore, a detailed chemistry approach is necessary to analyze combustion.

Adaptation of the chemical mechanism for engine modelling can be obtained by two different methodologies which are direct integration of chemistry where the online solution of species reaction and diffusion equations necessary, and tabulation of the chemistry where tables are used to store results that are obtained by reaction-diffusion equations. The time reduction for direct integrated chemistry approach by decreasing number of species in the chemical mechanism; however, it will result of lack of accuracy. Thus, the significant advantage of tabulation is the reduction of CPU time by solving detailed chemical mechanism at the same time.

Characterization of the combustion process and validation of different computational models to predict combustion accurately is the focus of this study. Combustion models are developed by Politecnico Di Milano Internal Engine Group and simulations are performed to validate reliability of these models. OpenFoam which is strong, free and Linux based open source CFD tool is used to practice simulations by adapting Lib-ICE applications and libraries which is developed by Polimi-ICE Group; furthermore, necessary experimental validation is done by data which are provided by Engine Combustion Network of Sandia National Laboratories for. In addition to analysis of different combustion models, soot prediction is also one of the considerations of this study where a specified combustion model is used to estimate soot formation behavior under different operating conditions. Finally, an alternative fuel dimethyl ether is tested with respect to conventional diesel fuel n-dodecane.

Different chemical mechanisms and combustion models which are Representative Interactive Flamelet (RIF) Model, Tabulated Well-Mixed (TWM) Model, Tabulated Representative Interactive Flamalet (TRIF) Model and finally Approximated Diffusion Flamelet (ADF) Model are tested. Simulations are initially performed by RIF model to exercise behavior of varied chemistry and then combustion models are analyzed under various circumstances. Although the study mainly concentrates on RIF and TWM models, a comprehensive comparison of all combustion models is provided.

In the next chapters, the theory of combustion process, modelling techniques and comparison of combustion models by means of heat release rate and other significant parameters are discussed.

The thesis contains six chapters:

- Chapter 1 contains explanation of the theory of compression ignition combustion process by considering emissions and regulations.

- Chapter 2 explains the basis of Computational Fluid Dynamics, which is a computer-based simulation method, in order to analyze fluid flow by solving set of differential equations, and application of CFD into combustion process.

- Chapter 3 describes the application methodology of chemical mechanism into combustion models.

- Chapter 4 includes experimental and simulation setup, which includes numerous operating conditions, for computational models.

- Chapter 5 contains the validation of different chemical mechanisms and several combustion models by main combustion characteristic curves.

- Chapter 6 gives conclusion and further possible suggestions to improve the outcomes of this study.

Chapter 1

Diesel Engine Combustion Process

Internal combustion engines are machines used to convert energy obtained by combustion into mechanical energy. Main classification in internal combustion engine is related to type of combustion process which are spark ignition engines and compression ignition engines. Compression ignition engine refers to diesel engine and it is the subject of this study. As written above, combustion process is the main parameter to obtain useful shaft work. In this chapter, diesel combustion will be explained in detail by including emissions and emission standards.

1.1 Description of Diesel Combustion

The combustion process in a diesel engine is based on compression ignition of heterogenous mixture since atomization of liquid state fuel into small droplets is occurred in air inside of the cylinder and this process also called as non-premixed combustion. Thus, there is no pre-mixed charge until beginning of combustion due to different physical state of the reactants.

The combustion chamber is fed by only air during the induction period and compression of air occurs within the compression stroke. The liquid fuel is injected at high velocities into the cylinder which contains air at sufficiently high temperature and pressure; furthermore, within the cylinder which can be stated as combustion chamber as well, a mixing process starts to occur between air and vaporized small fuel droplets. This circumstance creates a local premixed charge; moreover, it leads to auto-ignition of some elements of this mixture due to high pressure and temperature. As seen from the figure (Fig. 1.1), the core of the spray involves the liquid fuel droplets and relatively small variation of vapor. Air is at

the outer areas and it results breaking of the droplets into smaller ones. In addition to this, air helps the evaporation process of liquid fuel since it has higher temperature compared to injected fuel due to compression process. A cloud of air-fuel come into existence on the downstream part by air motion even though the central core of the spray has sufficient momentum to preserve its shape. The fuel-air ratio becomes rich at the central part of spray center and leaner toward air side of the spray. Auto-ignition occurs at some local points where the local fuel-air ratio close to the stoichiometric condition. In general, the process is mainly related to local conditions; hence, it can be stated that the process is independent from the overall air-fuel ratio of the charge. Although there are many factors affecting the rate of heat release, it is controlled mainly by the mixing process of air with fuel vapor.

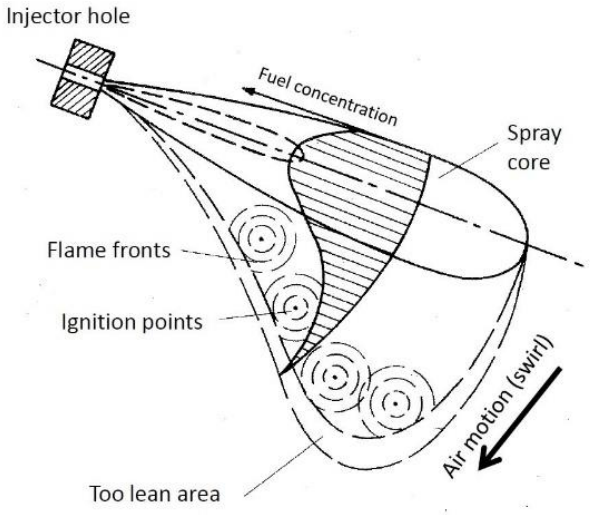

Figure 1.1: Spray evolution and ignition scheme [1]

In order to obtain a better combustion, turbulence has to be taking into consideration due to mixing phenomena between air and fuel since mixing rate is several times more than molecular diffusion rate. Therefore, organized charge motions are used to increase fuel evaporation, mixing between air/fuel and mixing between burned gases/air to decrease soot formation with better oxidation process. There are three methods which are swirl, tumble and squish to obtain organized charge motions. Swirl is the rotational flow with respect to the cylinder axis and it can be achieved by shrouded valve, direct port or helical port to create turbulence to enhance turbulent flame speed. Tumble has the same aim with swirl motion and it is used when swirl motion is not adequate due to symmetry of

cylinder head, for instance four-valve, pent-roof combustion chamber. Although it is generated during the intake stroke with respect to cylinder axial plane, the effect is increased in the compression stroke. Finally, the squish is a process that generates rotational motion on cylinder axial plane near the end of compression stroke with the aid of non-uniform structure of combustion chamber. The following figure represents the theory of swirl, tumble and squish methods respectively.

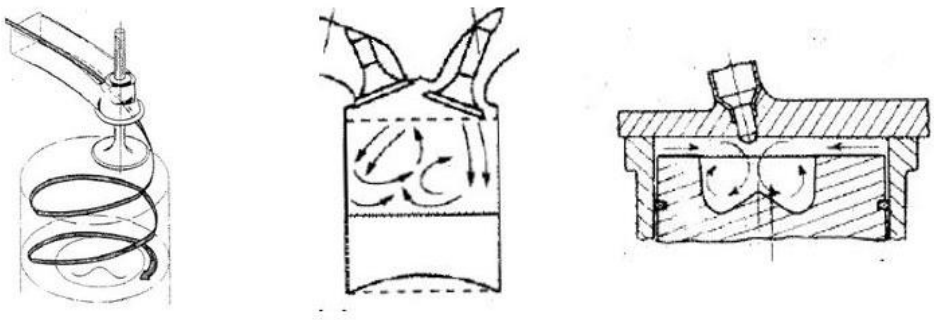

Figure 1.2: Swirl, Tumble and Squish motion respectively

In more detail, the diesel combustion process has four phases [5] which can be seen from the Fig. 1.3, where *SOI* and *EOI* refer to start of injection and end of injection respectively. Fig. 1.3 represents the phases with respect to crank angle degrees. The initial phase is called as ignition delay which occurs between the region *a-b*. It defines an interval between start of the fuel injection inside the cylinder and beginning of combustion process. Furthermore, it ends with the first energy release. This process induces to second phase of the combustion process which is called as premixed combustion. It covers the region between *b-c* and it is also defined as rapid combustion. Within this phase, a rapid combustion of premixed air-fuel charge occurs. This process produces very steep curve of energy release rates and consequently a rapid increment of cylinder pressure. The third phase is mixing-controlled combustion which happens between *c-d*. In this phase, diffusion process takes significant role since burning rate is controlled by the mixing process between air and the fuel. The time required for the chemical process are smaller compared to time for evaporation and diffusion; besides, the rate of heat release curve is controlled by the fuel injection rate within this range. The final phase which includes the region between *d* and *e* is late combustion which expresses the combustion of remaining air-fuel mixture and products of partial oxidation. The heat release rate curve has a continually decreasing trend in this phase.

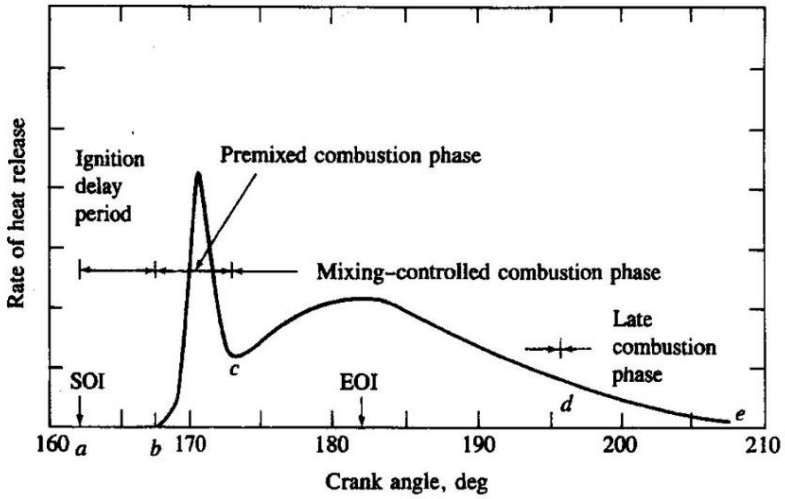

Figure 1.3: Combustion phases of diesel engine [5]

Ignition delay period contains physical processes that are fuel atomization, fuel vaporization and the diffusion of the fuel vapor in air; furthermore, chemical processes which are thermal cracking of large hydrocarbon molecules, partial oxidation reactions and start of chain reactions. While Fig. 1.4 shows the ignition delay period, the Fig. 1.5 represents the physical and chemical process in detail which lead to ignition delay. As shown in Fig. 1.4, ignition delay has two components where the first part symbolizes the physical process which is combustible mixture preparation and the second part indicates chemical process that results auto-ignition.

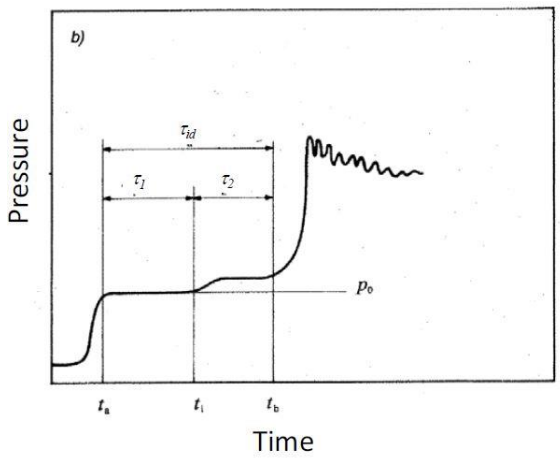

Figure 1.4: Representation of ignition delay

The time for ignition delay can be explained as:

$$\tau_{id} = A \times p^n \times exp(E_a/RT) \tag{1.1}$$

Where τ_{id} is total ignition delay, p is pressure and T is temperature. A, n and E_a are parameters which depend on fuel.

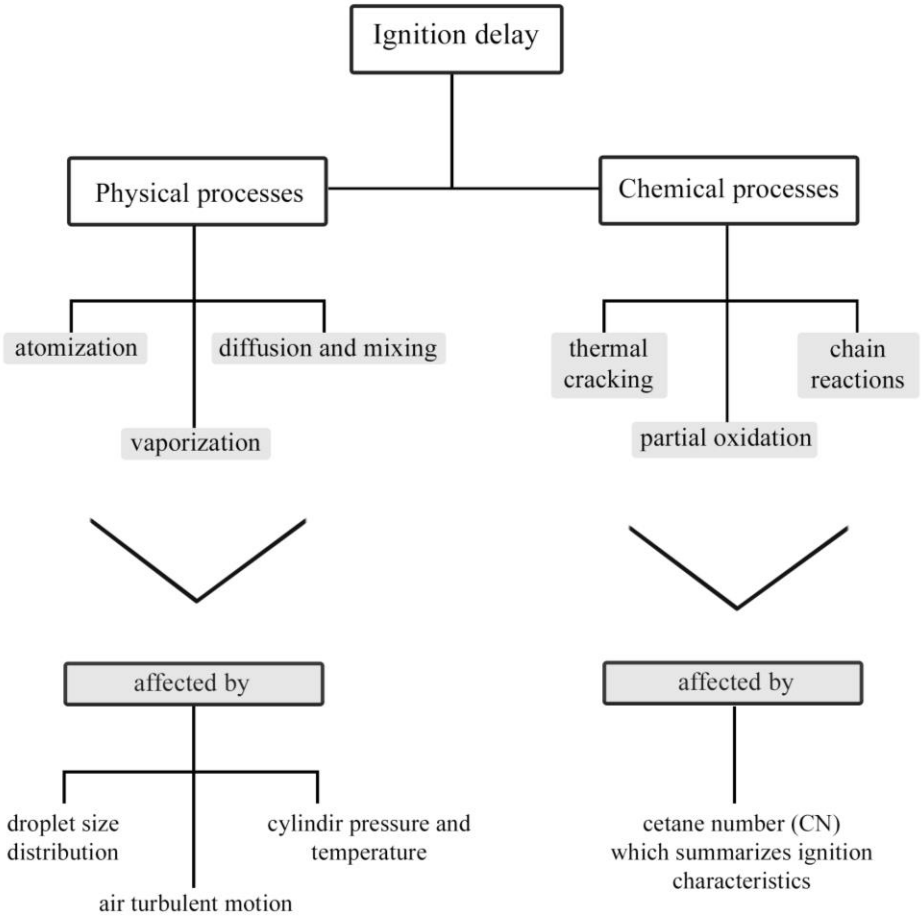

Figure 1.5: Ignition delay process and factors affecting process

1.2 Emissions and Regulations

1.2.1 Emissions

Emissions from automotive engines have significant impacts on air pollutions in urban areas since operation of an internal combustion engine based on combustion and discharge process of burned gasses and particles which promotes to global warming, smog, acid rain and other health problems. Even though the amount of pollution from one vehicle is very low, overall contribution from vehicles are quite high.

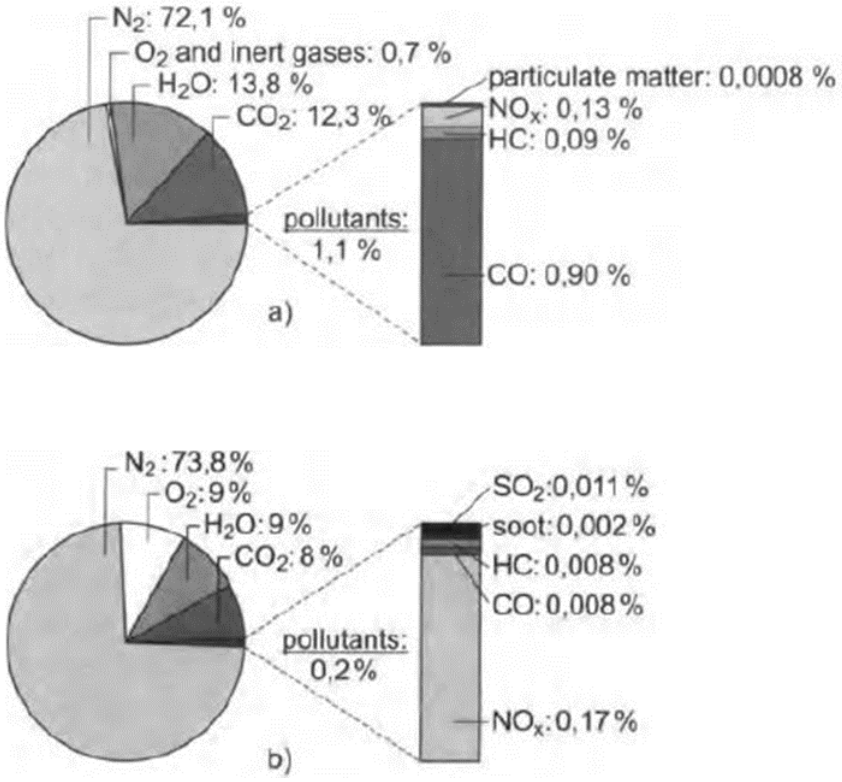

Figure 1.6: Exhaust emissions composition (by volume fraction) for spark ignition engines (a) and diesel engines (b) [4]

The primary reasons for emissions are non-stoichiometric combustion process, dirtiness and disintegration of nitrogen within the combustion chamber. Main contributions from internal combustion engines are Carbon Monoxide (*CO*), Unburned Hydrocarbons (*HC*), Particulate Matter (*PM*) or soot, Nitrogen Oxides (NO_x), Sulphur Oxides (SO_2 and SO_3) and Carbon Dioxide (CO_2). Our main consideration is emissions from diesel engines of commercial vehicles instead of all engine types. A representation of the emission from a diesel engine is given with respect to temperature zones and equivalence ratio (Fig.1.7).

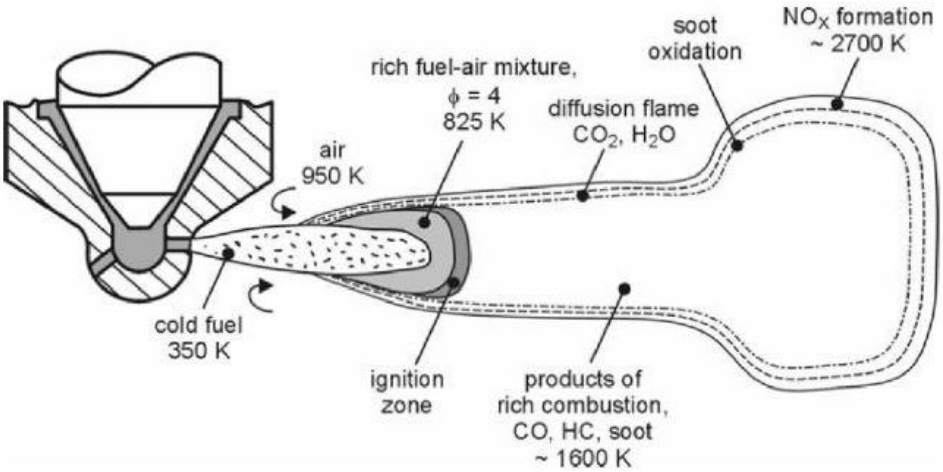

Figure 1.7: Diesel emissions related to temperature and equivalence ratio [1]

In diesel engine, soot emissions which is occurred due to incomplete combustion of fuel hydrocarbons have to be considered particularly; since, it has significant harmful effects on carcinogenic and mutagenic effects especially on bronchi and lungs in addition to environmental impacts. Soot formation has several stages which are fuel to precursors, precursors to primary nuclei, surface growth and oxidation step by step (Fig. 1.8). In the central region of fuel spray, precursors take shape. Primary nuclei formation occurs due to reaction between precursors and unsaturated hydrocarbons with hydrogen. Then, nuclei or spherules come into existence because of interaction between primary nuclei and chemical species which are rich in terms of carbon. Nuclei continues to grow up by collision, coagulation and aggregation. The oxidation process converts the precursors, nuclei and particles into carbon monoxide or carbon dioxide if there is sufficient time, concentration of oxidizing species and temperature [1].

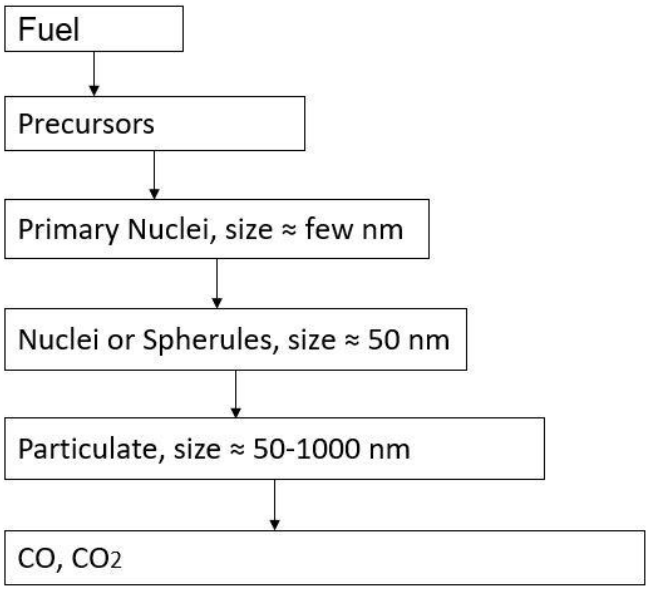

Figure 1.8: Scheme of soot formation

Soot particles can be classified in three sub-categories:

- Single nuclei: diameter of the soot particle is less than 50 nm. They have the largest number as quantity; nevertheless, their mass does not have a significant value.

- Particles: when the diameter of the soot particle between 50 nm and 1000 nm, it is called as particles. They are important in terms of mass contribution.

- Agglomerates: it refers the soot particles whose diameter are more than 1000 nm. They are not produced directly within the combustion process, they are formed by deposits on combustion chamber surfaces and/or valves. Even though their quantity is very low, they can have a little impact on normalized mass-weighted diameters.

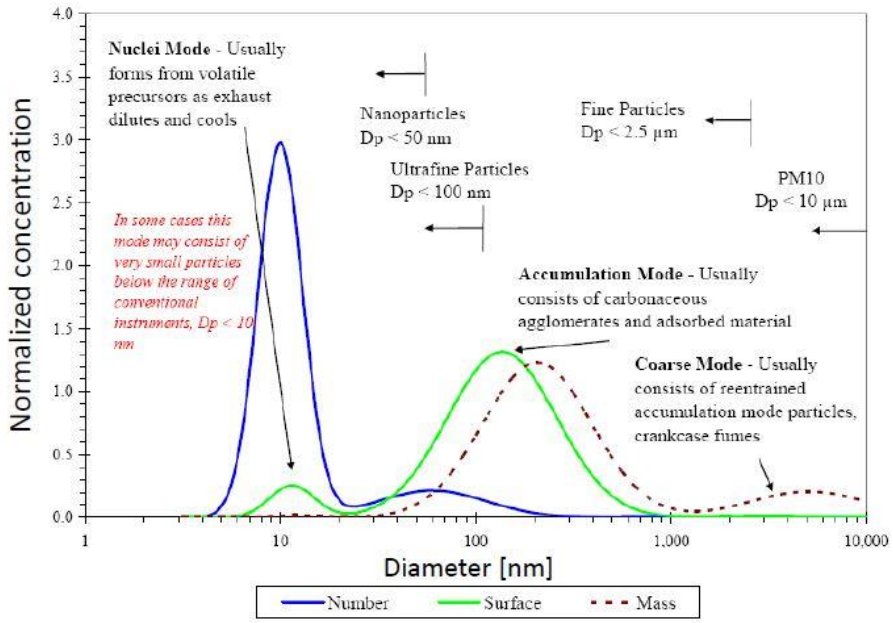

Figure 1.9: Soot particles distributions [1]

Emission control in diesel engines can be obtained by two approach which are during the combustion process and after the combustion process. [1, 5] The scope is trying to decrease the pollutant emissions within the combustion process; otherwise, eliminate toxic ingredients after their formation. While method for after the combustion is that optimizing the exhaust gases with after treatment systems, methods for during the combustion are:

- Optimizing the fuel according to quality of exhaust gases that considers the reduction of pollution.

- Mixture preparation optimization to control air/fuel ratio in all operating conditions.

- Combustion optimization to increase the speed and to make process more complete.

Therefore, simply the methods of controlling the emission inside the combustion chamber are usage of recycled exhaust gases to dilute the charge and reduce the amount of NO_x emission, multiple injections to optimize the process for better combustion, combustion chamber design to augment mixing and usage of diesel fuel with high characteristics such as high cetane number and low density. The first consideration is related to particulate matter and nitrogen oxide emissions. To control the emissions during the combustion process has some negative effects

due to balance between particulate emission (soot), NO_x emission and fuel consumption efficiency since the method which decreases the soot emission mostly leads to increase of fuel consumption and nitrogen oxides emissions. Because of that, some soot formation is generally accepted to keep fuel consumption at a certain level in combustion process and after-treatment procedure such as diesel particulate filter (DPF) and selective catalytic reduction (SCR) is applied to clean exhaust gases from soot particles and nitrogen oxides. The second consideration is related to carbon monoxide and carbon dioxide emissions. Normally *CO* is originated in rich mixture region; nevertheless, due to availability of high amount of oxygen and lean overall operating conditions in diesel engines, most of the *CO* are oxidized to CO_2 within the combustion chamber. Thus, the amount of *CO* is negligible and CO_2 emission should be controlled by virtue of impact on global warming and direct linkage between fuel consumption.

1.2.2 Regulations

Emission Regulations are based on the types of engine and their application areas. There are two methodology which are New European Driving Cycle (NEDC) and Worldwide Harmonized Light Vehicle Test Cycle (WLTC) for testing procedure. The NEDC is the older methodology and all new cars have to be tested with WLTC from September 2018 [27]. The NEDC cycle is subdivided into two subcategories that are urban and extra urban; besides, The WLTC cycle has four separated region which are low, medium, high and extra high cycles. The comparison between NEDC and WLTC regarding speed and time can be seen from the Fig. 1.10 and 1.11.

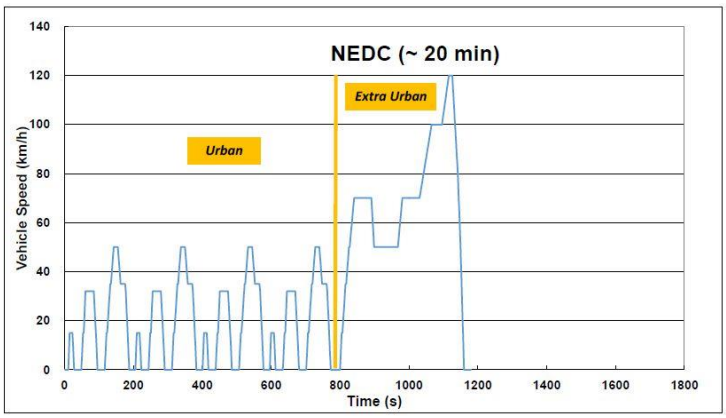

Figure 1.10: New European Driving Cycle Test Cycle [27]

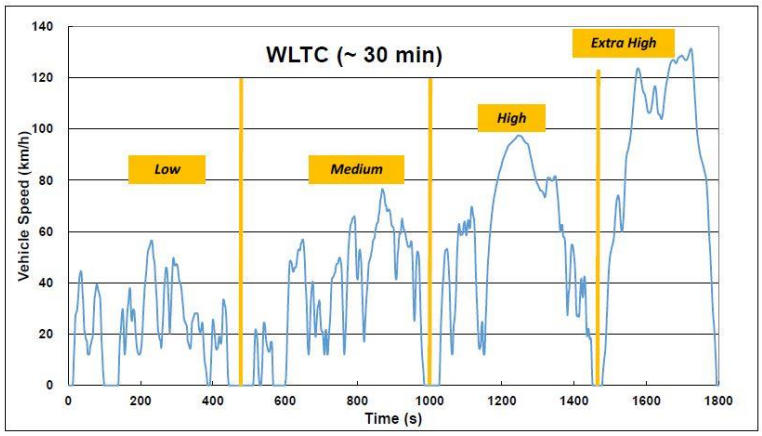

Figure 1.11: Worldwide harmonized light duty vehicle test cycle (Class 3) [27]

In addition to these tests, Real Driving Emission (RDE) test which has urban, extra urban and highway periods is used to measure pollutants that emitted by cars during real driving condition. This method is a complementary procedure to confirm laboratory tests. In the Tab. 1.1 and 1.2, the emission regulation for Europe from past to today are given [28]; furthermore, the future trend of the emissions is stated as "Further pollutant emission regulation in the sense of Euro 7 is not planned for the moment. There may be an opportunity for the next step of emission regulation with the introduction of post-2020 CO_2 regulations" [27].

	NOx [mg/kg]	**THC [mg/km]**	**THC+NOx [mg/km]**	**PM [mg/km]**	**PN [#/km]**
Euro 1	-	-	970	140	-
Euro 2	-	-	900	80	-
Euro 3	500	-	560	50	-
Euro 4	250	-	300	25	-
Euro 5a	180	-	230	5	-
Euro 5b	180	-	230	5	6x10e11
Euro 6	80	-	170	5	6x10e11

Table 1.1: Emission standards for diesel passenger cars on NEDC

	NOx [g/kWh]	THC [g/kWh]	PM [mg/kWh]	PN [#/kWh]
Euro 1	8	1.23	360	-
Euro 2	7	1.1	250	-
Euro 3	7	1.1	150	-
Euro 4	5	0.66	100	-
Euro 5a	3.5	0.46	20	-
Euro 5b	2	0.46	20	-
Euro 6	0.4	0.13	10	6x10e11

Table 1.2: Emission standards for diesel heavy-duty vehicles on NEDC

where *THC* is total hydrocarbons, *PM* is particulate matters and *PN* is the particulate number.

The CO_2 emission standard is defined as 130 g/km until 2019 and no more than 95 g/km as a target in 2020 (defined for NEDC cycle) for average car in Europe [27].

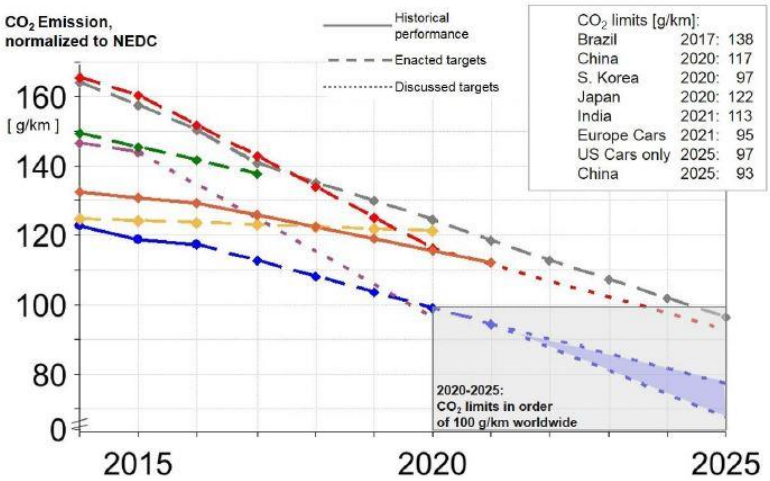

Figure 1.12: Historic CO2 emissions and targets for different world regions [27]

Chapter 2

Fundamentals for Modeling

Combustion modeling has substantial advantages compared to experimental process since they are more cost effective and time saving. Although there are many models for combustion process considering its various application range, three different models which are zero-dimensional thermodynamic model, quasi-dimensional models and multi-dimensional models that is also called as CFD codes, are discriminated. This chapter explains the basis of computational fluid dynamics or briefly CFD which is the computer-based simulation technique that analyze fluid flow, heat transfer and related subjects by solving set of differential equations for conservation of mass, momentum and energy, and application of CFD into combustion process.

2.1 Conservation Equations

Computational Fluid Dynamics (CFD) modelling is based on conservation laws which indicates that the variation of a quantity inside a domain is equal to equilibrium between entering and exiting quantity in addition to source contribution which generates this quantity. This principle is applied for mass, momentum and energy equations for a given fluid problem. In internal combustion engine modelling with direct injection, additional transport or source terms must be taken into consideration due to two phase flows with evaporating fuel droplets within the cylinder [4].

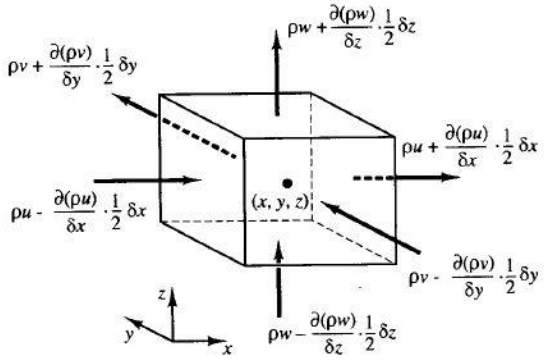

Figure 2.1: Mass flow within control volume [6]

2.1.1 Mass Conservation

Mass conservation can be also stated as continuity equation and it is referred to a scalar property density, ρ. The continuity equation is obtained from volume of an infinitely small element and can be written in general form as:

$$\frac{\partial \rho}{\partial t} + \vec{\nabla}.\left(\rho \vec{U}\right) = 0 \tag{2.1}$$

2.1.2 Momentum Conservation

Momentum equation expresses the momentum change inside a domain by sum of external forces on the control volume. It is referred to a vectoral property $\rho\vec{U}$, and it is derived for three cartesian coordinates. The momentum equation in general:

$$\frac{\partial\left(\rho \vec{U}\right)}{\partial t} + \vec{\nabla}.\left(\rho \overrightarrow{UU} + p\bar{\bar{I}} - \bar{\bar{\tau}}\right) = \rho \overrightarrow{f_e} \tag{2.2}$$

where $-p\bar{\bar{I}}$ is the isotropic pressure component, $\overrightarrow{f_e}$ is the external volume forces and $\bar{\bar{\tau}}$ is the viscous shear stress tensor that stand for the internal friction force within the fluid layers. By defining the μ as dynamic viscosity and δ_{ij} as Kronecker delta, viscous shear tensor, $\bar{\bar{\tau}}$ can be expressed as:

$$\bar{\bar{\tau}} = \mu\left[\left(\frac{\partial U_j}{\partial x_i} + \frac{\partial U_i}{\partial x_j}\right) - \frac{2}{3}\left(\vec{\nabla}.\vec{U}\right)\delta_{ij}\right] \tag{2.3}$$

2.1.3 Energy Conservation

Energy conservation equation which depends on the first law of thermodynamic can be written in terms of total energy per unit mass which is equal to fluid internal energy plus its kinetic energy. However, it is more useful to state energy equation with respect to enthalpy for combustion process. The energy equation in general form can be written as:

$$\frac{\partial(\rho h)}{\partial t} + \vec{\nabla}.\left(\rho h\vec{U} - k\vec{\nabla}T - \bar{\bar{\tau}}\vec{U}\right) = \frac{\partial p}{\partial t} + \rho\overrightarrow{f_e} \cdot \vec{U} + q_H \tag{2.4}$$

where k is the thermal conductivity, q_H is the heat source and $\rho\overrightarrow{f_e} \cdot \vec{U}$ is the work of volume force.

2.2 Numerical Methodology and Turbulence Model

There are three numerical methodology which are Direct Numerical Simulation (DNS), Large Eddy Simulation (LES) and Reynolds-Averaged Navier-Stokes Equations (RANS) to solve Navier-Stokes equations in general for laminar and turbulent flows. Although, DNS solves the smallest length scales that are defined by the size of smallest eddies (also called Kolmogorov length scale) of the fluid dynamic problem, LES only solves the large scale of eddies and described the behavior of smaller eddies by semi-empirical sub-models. Besides, RANS is the highest-level approximation and it splits the quantities by averaged and fluctuating values. Due to averaging process in RANS, two additional terms which are turbulent shear and turbulent flux are added into set of conservation equations [4]. Reynolds Averaging procedure is simply explained below.

$$\varphi = f(t) = \bar{\varphi} + \varphi' \tag{2.5}$$

$$\bar{\varphi} = \frac{1}{t}\int_0^t f(t)dt \tag{2.6}$$

$$\bar{\varphi}' = 0 \tag{2.7}$$

where $\bar{\varphi}$ is the mean quantity and φ' time dependent fluctuating component of $f(t)$. For a compressible flow problem, Favre averaging (mass-weighted) procedure is applied instead of Reynolds averaging. Favre averaging can be stated as:

$$\varphi = f(t) = \tilde{\varphi} + \varphi' \tag{2.8}$$

$$\bar{\varphi} = \frac{1}{t}\int_0^t f(t)dt \tag{2.9}$$

$$\tilde{\varphi} = \frac{\overline{\rho\varphi}}{\bar{\rho}} \tag{2.10}$$

$$\tilde{\varphi}' = 0 \tag{2.11}$$

Comparison between DNS, LES and RANS approach are shown in the Fig. 2.2.

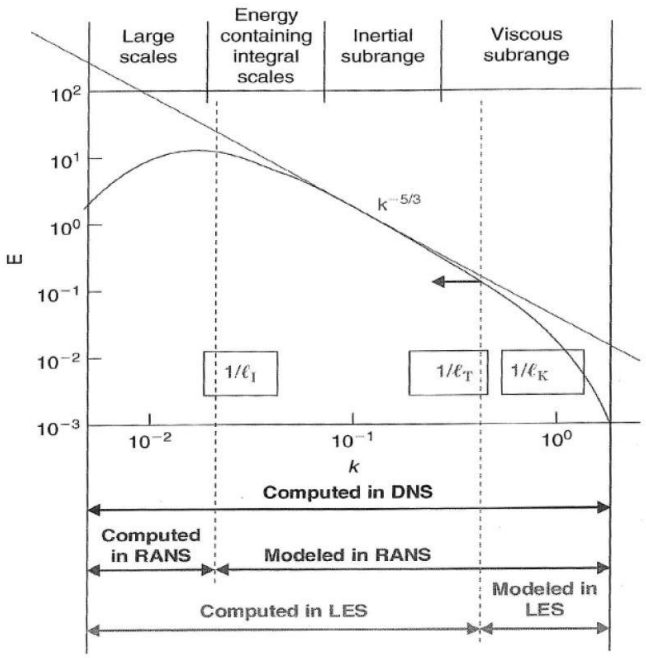

Figure 2.2: Comparison of different numerical methodologies

In the RANS model the turbulent behavior of the flow field is contained in the turbulent shear (Reynolds) stress and in the turbulent diffusivities which are obtained as time-averaged quantities. Turbulent viscosity has the same unit with molecular viscosity and it is expressed as:

$$\mu_t = C_\mu \cdot \rho \cdot l \cdot q \tag{2.12}$$

where C_μ is a constant, q is the characteristic velocities and l is the characteristic length scales.

Although there are several models to determine turbulence effect, only k-ε model is considered within this study. k-ε model is a two-equation turbulence model based on turbulent kinetic energy, k and its dissipation rate, ε. Turbulent viscosity is derived from turbulent kinetic energy and dissipation, then turbulent length and velocity scales are derived from turbulent scale.

$$k = \frac{1}{2}\overline{U_i' U_i'} = \frac{1}{2}(\overline{U_1'^2} + \overline{U_2'^2} + \overline{U_3'^2}) \tag{2.13}$$

$$\varepsilon = \frac{k^{3/2}}{l} \tag{2.14}$$

$$\mu_t = C_\mu \cdot \rho \cdot l \cdot \sqrt{k} \tag{2.15}$$

A balance equation is solved to evaluate turbulent kinetic energy, k and a second transport equation is solved to obtain dissipation rate, ε.

$$\frac{\partial k}{\partial t} + \overline{U_i'}.\frac{\partial k}{\partial x_i} = \frac{\partial}{\partial x_i}\left(\frac{\mu_t}{\rho C_k}\frac{\partial k}{\partial x_i}\right) + \frac{\mu_t}{\rho}\frac{\partial \overline{U_j'}}{\partial x_i}\left(\frac{\partial \overline{U_j'}}{\partial x_i}\frac{\partial \overline{U_i'}}{\partial x_j}\right) - \varepsilon \tag{2.16}$$

$$\frac{\partial \varepsilon}{\partial t} + \overline{U_i'}.\frac{\partial \varepsilon}{\partial x_i} = \frac{\partial}{\partial x_i}\left(\frac{\mu_t}{\rho C_\varepsilon}\frac{\partial \varepsilon}{\partial x_i}\right) + \frac{\mu_t}{\rho}\frac{\partial \overline{U_j'}}{\partial x_i}C_1\frac{\varepsilon}{k}\left(\frac{\partial \overline{U_j'}}{\partial x_i}\frac{\partial \overline{U_i'}}{\partial x_j}\right) - C_2\frac{\varepsilon^2}{k} \tag{2.17}$$

C_μ, C_ε, C_k, C_1, C_2 are the constants and their values must be specified according to problem; however, their recommended values [4] are given in the Tab 2.1. Furthermore, by combining equation 2.14 and 2.15 we obtain:

$$\mu_t = C_\mu \cdot \rho \cdot \frac{k^2}{\varepsilon} \tag{2.18}$$

C_μ	C_ε	C_k	C_1	C_2
0.09	1.3	1.0	1.44	1.92

Table 2.1: Recommended values for empirical constants C_i

Usage of k-ε model is favorable far away from the wall region; however, near the wall region singularity occurs due to $\frac{\varepsilon^2}{k}$ term. To avoid incorrect estimations, wall-functions should be implemented where the results near the wall region are important.

2.3 Implementation of Conservation Equations to In-Cylinder Applications

Additional source (transport) terms must be taken into account to describe heat transfer between liquid and gaseous phase due to two phase flows as well as heat released by chemical reactions within the cylinder [4]. Small index "m" defines every species in the cylinder. Consequently, the mass, momentum and the energy equations are express respectively below.

$$\frac{\partial \rho_m}{\partial t} + \frac{\partial \rho_m U_i}{\partial x_i} = \frac{\partial}{\partial x_i}\left(\rho D \frac{\partial(\frac{\rho_m}{\rho})}{\partial x_i}\right) + \dot{\rho}_m{}^s + \dot{\rho}_m{}^c \qquad (2.19)$$

$$\frac{\partial(\rho U_j)}{\partial t} + U_j \frac{\partial(\rho U_j)}{\partial x_i} = -\frac{\partial p}{\partial x_j} + \frac{\partial \tau_{ij}}{\partial x_i} + \rho F_j^s + \rho g_j\,; \quad j = 1,2,3 \qquad (2.20)$$

$$\rho c_p \frac{\partial T}{\partial t} + U_i \frac{\partial T}{\partial x_i} = k \frac{\partial^2 T}{\partial x_i{}^2} + \frac{\partial}{\partial x_i}\left(\rho D \sum_m h_m \frac{\partial(\frac{\rho_m}{\rho})}{\partial x_i}\right) + \rho\varepsilon + \dot{Q}^s + \dot{Q}^c \qquad (2.21)$$

D represents the mass diffusion, while s terms are source terms due to spray effects and c terms are source terms due to combustion. "j" defines the spatial dimensions for momentum conservation equations. ρF_j^s represents the

momentum increase of the gas phase by virtue of spray process and gravity only acts in the vertical direction since $g_1 = 0$, $g_2 = 0$ and $g_3 = g$. The term $\rho\varepsilon$ refers to dissipation of turbulent kinetic energy while $\dot{Q}^s$ and $\dot{Q}^c$ are the source terms.

Furthermore, different combustion models that are used in this study are discussed in Chapter 3.

Chapter 3

Combustion Models

Diesel combustion deals with multi-phase flow, auto ignition of fuel and diffusion flame structure. Therefore, it is essential to pay attention chemical mechanism and chemistry-turbulence interaction to estimate a reliable outcome for combustion process. This chapter includes the application of chemistry into combustion models and differences between combustion models. The chemical kinetics can be adopted in two different ways which are direct integration and tabulation. Within the first methodology, reaction-diffusion equations for any species contained in the chemical mechanism are solved during the simulation. The most widely used direct integration methods are Representative Interactive Flamelets (RIF) and Well-Mixed approach [23]. The main difference between RIF and Well-Mixed Model is that the RIF model accounts for turbulence-chemistry interaction while Well-Mixed Model does not. The second methodology refers to usage of tabulation instead of a direct integration of chemistry. The primary cause of usage of tabulation is the reduction of required CPU time. The idea behind the tabulation is that storing the results obtained from reaction-diffusion equations to be taken during the simulation. The simulations are based on RIF, Tabulated RIF (TRIF) which is RIF model with tabulated reaction rates, Tabulated Well-Mixed Model (TWM) and Approximated Diffusion Flamelet (ADF) approach; furthermore, they will be explained in detail in next sections.

3.1 Direct Integration of Chemistry

In this part of the thesis, Representative Interactive Flamelet, RIF model is discussed.

3.1.1 Flamelet Model Concept

The significant fraction of the chemical reactions occurs in thin layers which can be said as stretched counter-flow laminar reaction sheets and these laminar reaction sheets are called as flamelets [42,43]. A schematic representation of the flamelet approach is represented in Fig. 3.1. The overall turbulent flame can be stated as ensemble of multiple laminar flamelets.

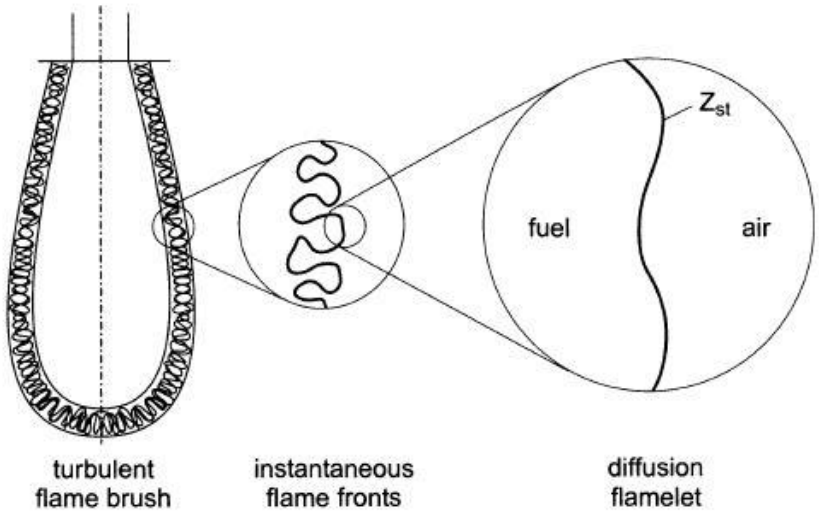

Figure 3.1: Representation of flamelet concept [4]

Within this thin layer, the chemistry is fast in proportion to diffusion and convection process. Within flamelet region, combustion is one-dimensional process and depends only local mixture fraction *Z* which is the ratio between fuel and oxidizer. The *Z* value is within the range between zero and one and it is proportional to mass fraction of the fuel and oxidizer.

$$Z = \frac{\dot{m}_{fuel}}{\dot{m}_{fuel} + \dot{m}_{oxidizer}} \tag{3.1}$$

The simulation is sub-divided into two sub-domains which are physical and chemical ones. While the three-dimensional turbulent flow equations for mixture fraction and transport equation are solved in physical domain, the one-dimensional flamelet equations which depend on mixture fraction and scalar

dissipation rate, χ are solved in chemical domain. The Fig. 3.2 illustrates the flamelet approach for turbulent non-premixed combustion simply.

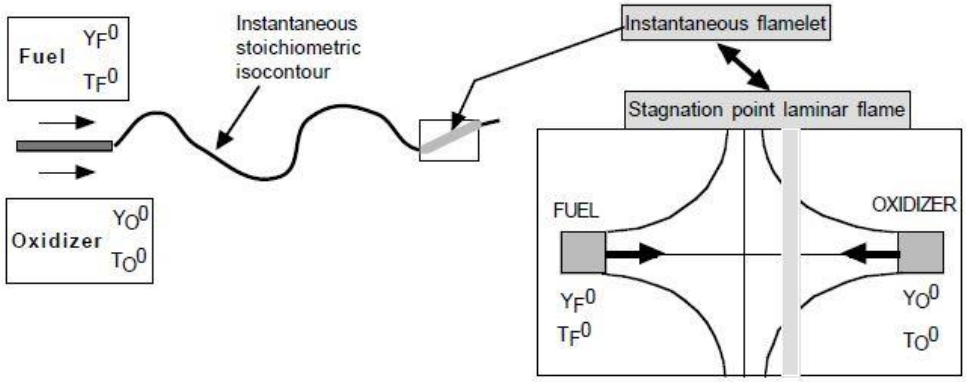

Figure 3.2: Flamelet approach for turbulent non-premixed combustion [3]

3.1.2 Laminar Diffusion Flame Equations

Under several assumptions, the idealized flame is analyzed. The assumptions are:

- Low Mach number
- Constant pressure
- All species diffusion coefficients are same and equal to *D*
- All species heat capacities are same and equal to c_p

The steps to obtain laminar diffusion flame equations are described [3, 4]. Initially, the chemical reaction for fuel and oxidizer can be simply written as:

$$v_F F + v_O O \leftrightarrow v_P P \tag{3.2}$$

Before writing down the conservation equations for fuel (*F*), oxidizer (*O*) and temperature (*T*), some relations and definitions are explained. The relation between fuel/oxidizer and fuel/temperature reaction rate is:

$$\dot{\omega}_O = s\dot{\omega}_F \; where \; s = \frac{v_O W_O}{v_F W_F} \quad and \quad \dot{\omega}_T = Q\dot{\omega}_F \tag{3.3}$$

where $\dot{\omega}$ is the reaction rate, s is the mass stoichiometric ratio and Q is the heat release per unit fuel mass. Thus, the conservation equation is written below.

$$\frac{\partial \rho Y_F}{\partial t} + \frac{\partial (\rho U_i Y_F)}{\partial x_i} = \frac{\partial}{\partial x_i}\left(\rho D \frac{\partial Y_F}{\partial x_i}\right) + \dot{\omega}_F \tag{3.4}$$

$$\frac{\partial \rho Y_O}{\partial t} + \frac{\partial (\rho U_i Y_O)}{\partial x_i} = \frac{\partial}{\partial x_i}\left(\rho D \frac{\partial Y_O}{\partial x_i}\right) + s\dot{\omega}_F \tag{3.5}$$

$$\frac{\partial \rho T}{\partial t} + \frac{\partial (\rho U_i T)}{\partial x_i} = \frac{\partial}{\partial x_i}\left(\frac{\lambda}{c_p}\frac{\partial Y_F}{\partial x_i}\right) - \frac{Q}{c_p}\dot{\omega}_F \tag{3.6}$$

Assuming unity Lewis number ($Le = \frac{\lambda}{\rho c_p D} = 1$) [42] which shows the relation between thermal and mass diffusivity and combining equations 3.4, 3.5 and 3.6, three conserved scalars obtained.

$$z_1 = sY_F - Y_O \tag{3.7}$$

$$z_2 = \frac{c_p T}{Q} + Y_F \tag{3.8}$$

$$z_3 = s\frac{c_p T}{Q} + Y_O \tag{3.9}$$

z stands for all scalars, and the balance equation without source terms for z is given as:

$$\frac{\partial \rho z}{\partial t} + \frac{\partial (\rho U_i z)}{\partial x_i} = \frac{\partial}{\partial x_i}\left(\rho D \frac{\partial z}{\partial x_i}\right) \tag{3.10}$$

As seen from the equation above, the changes are related to convection and diffusion instead of combustion reactions. The boundary conditions for the z_1, z_2

and z_3 are given in the Tab. 3.1 with respect to mass fraction of fuel and oxidizer in fuel and oxidizer stream, ${Y_F}^0, {Y_O}^0$.

	Fuel Value Z_i^F	**Oxidizer Value Z_i^O**
z_1	$s{Y_F}^0$	$-{Y_O}^0$
z_2	$\frac{c_p T_F^0}{Q} + {Y_F}^0$	$\frac{c_p T_O^0}{Q}$
z_3	$s\frac{c_p T_F^0}{Q}$	$s\frac{c_p T_O^0}{Q} + {Y_O}^0$

Table 3.1: Boundary conditions for *z*

A normalization procedure is applied on z_1, z_2 and z_3 to have a value of 0 at the oxidizer side and value 1 at the fuel side. The normalized variable is shown as *z*; furthermore, the transport equation which used for z can be used also for Z.

$$Z_j = \frac{z_j - z_j^O}{z_j^F - z_j^O} \;\; where\; j = 1,2,3 \tag{3.11}$$

Due to same boundary conditions, Z_1, Z_2, Z_3 have same values and they are represented just by Z and it is called as mixture fraction. As mentioned before the flame structure can be considered as one-dimensional due to negligible effects of the gradients along the flame front with the assumptions of stoichiometric mixture and very thin flame front; therefore, it depends on time and normal to the flame front coordinate which is considered as Z. Fig. 3.3 represents the flame in the Z-space.

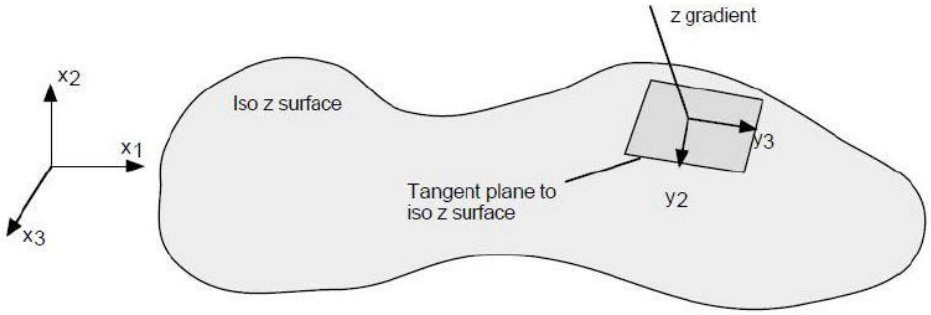

Figure 3.3: Flame structure in Z-space [3]

Thus, temperature and mass fraction reactions are only functions of time and Z.

$$Y_k = Y_k(Z,t) \tag{3.12}$$

$$T_k = T(Z,t) \tag{3.13}$$

Then the conservation equation for the species mass fraction can be written as:

$$\frac{\partial \rho Y_k}{\partial t} + Y_k\left(\frac{\partial \rho}{\partial t} + \frac{\partial(\rho U_i)}{\partial x_i}\right) + \frac{\partial Y_k}{\partial Z}\left[\rho\frac{\partial Z}{\partial t} + \rho U_i\frac{\partial Z}{\partial x_i} - \frac{\partial}{\partial x_i}\left(\rho D\frac{\partial Z}{\partial x_i}\right)\right] \tag{3.14}$$

$$-\rho D\left(\frac{\partial Z}{\partial x_i}\frac{\partial Z}{\partial x_i}\right)\frac{\partial^2 Y_k}{\partial Z^2} = \dot{\omega}_k$$

Then the equation becomes by simplification:

$$\frac{\partial \rho Y_k}{\partial t} = \dot{\omega}_k + \rho D\left(\frac{\partial Z}{\partial x_i}\frac{\partial Z}{\partial x_i}\right)\frac{\partial^2 Y_k}{\partial Z^2} = \dot{\omega}_k + \frac{1}{2}\rho\chi\frac{\partial^2 Y_k}{\partial Z^2} \tag{3.15}$$

A new term χ is appeared in the last formulation and it refers to scalar dissipation rate. It is the parameter that control mixing process due to regulation the gradient of Z. The unit of the χ is the inverse of the unit of time. The formula of scalar dissipation rate is that:

$$\chi = 2D\left(\frac{\partial Z}{\partial x_i}\frac{\partial Z}{\partial x_i}\right) \tag{3.16}$$

The equation for the temperature can be also written as:

$$\frac{\partial \rho T}{\partial t} = \dot{\omega}_T + \frac{1}{2}\rho\chi\frac{\partial^2 T}{\partial Z^2} \tag{3.17}$$

,

The temperature equation can be written in enthalpy form as well:

$$\frac{\partial \rho h_s}{\partial t} = \dot{\omega}_T + \frac{1}{2}\rho\chi\frac{\partial^2 h_s}{\partial Z^2} + \frac{dp}{dt} \tag{3.18}$$

Equations 3.15 and 3.17 for species mass fraction balance and temperature obtained finally are called as flamelet equations.

3.1.3 CFD and Flamelet Interaction

Flamelet equations are solved with one-dimensional mesh and the initialization of the flamelet equations is done in the mixture fraction space according to pure mixing solution which depend on the mass fractions on the fuel and air side. Mass fractions on the fuel and air side are treated as boundary conditions for the initialization process and they are kept constant. While air side represents CO_2, N_2, O_2 and H_2O, the fuel side only contains fuel. Consequently, the initial chemical species and temperature are expressed as:

$$Y_k(Z) = (1 - Z){Y_k}^O + Z{Y_k}^F \tag{3.19}$$

$$h_S\,(Z) \;=\; (1 - Z)h_S\,(T_{air}) + Z\;h_S\,(T_{fuel}) \tag{3.20}$$

temperature of the fuel side is fixed; however, the temperature profile of the air side changes with respect to pressure alteration in time. The local enthalpy is used to compute temperature in mixture fraction space.

In the flamelet methodology, all reacting scalars are functions of mixture fraction, Z. In the physical domain the transition is done by the probability density functions (PDF) which shows the possibility of existence of a particular flamelet

in the physical CFD domain. Furthermore, the turbulence mixing process is represented by the mean and variance values of mixture fraction. Variance gives information related to turbulence and mixing. While high variance means high turbulence and inhomogeneous mixture, low variance indicates that turbulent dissipation occurred, and it results more homogeneous composition compared to higher one. Transport equation of Favre averaged mixture fraction, Z must be solved for mean and variance composition of the mixture fraction to evaluate the probability density function which is position and time dependent inside the cylinder. The transport equations are:

$$\frac{\partial \bar{\rho}\tilde{Z}}{\partial t} + \frac{\partial (\bar{\rho}\tilde{U}_\iota \tilde{Z})}{\partial x_i} = \frac{\partial}{\partial x_i}\left(\frac{\mu}{Sc_{\tilde{z}}}\frac{\partial \tilde{Z}}{\partial x_i}\right) + \dot{\rho}^s \tag{3.21}$$

$$\frac{\partial \bar{\rho}\widetilde{Z''^2}}{\partial t} + \frac{\partial (\bar{\rho}\tilde{U}_\iota \widetilde{Z''^2})}{\partial x_i} = \frac{\partial}{\partial x_i}\left(\frac{\mu}{Sc_{\widetilde{Z''^2}}}\frac{\partial \widetilde{Z''^2}}{\partial x_i}\right) + \frac{2\mu}{Sc_{\widetilde{Z''^2}}}(\nabla \tilde{Z})^2 - \rho\tilde{\chi} \tag{3.22}$$

$\tilde{\chi}$ is the mean scalar dissipation rate [3] and it can be expressed as:

$$\tilde{\chi} = C_x \frac{\tilde{\varepsilon}}{\tilde{k}} \widetilde{Z''^2} \tag{3.23}$$

Schmit number, *Sc* for both equations are taken as 0.85, and C_x is taken as 2. Although, mean and variance of the mixture fraction distribution is calculated, it does not give sufficient data to compute Favre-averaged mass fraction of each species, $\tilde{Y}_k$ in the physical domain. To compute $\tilde{Y}_k$, the whole probability density functions must be known. Thus, the most often used presumed function β-PDF which is defined below, is implemented [3, 4].

$$\tilde{P}(z) = \frac{\Gamma(\alpha+\beta)}{\Gamma(\alpha)+\Gamma(\beta)} Z^{\alpha-1}(1-Z)^{\beta-1} \tag{3.24}$$

where:

$$\Gamma(a) = \int_0^\infty t^{a-1}\, e^{-t} dt \tag{3.25}$$

α and β is computed from $\tilde{Z}$ and $\widetilde{Z''^2}$ as below:

$$\alpha = \tilde{Z}\left(\frac{\tilde{Z}(1-\tilde{Z})}{\widetilde{Z''^2}} - 1\right) \tag{3.26}$$

$$\beta = (1-\tilde{Z})\left(\frac{\tilde{Z}(1-\tilde{Z})}{\widetilde{Z''^2}} - 1\right) \tag{3.27}$$

An illustration for the probability density function is given in the Fig. 3.4 where γ is equal to $\alpha/\tilde{Z}$.

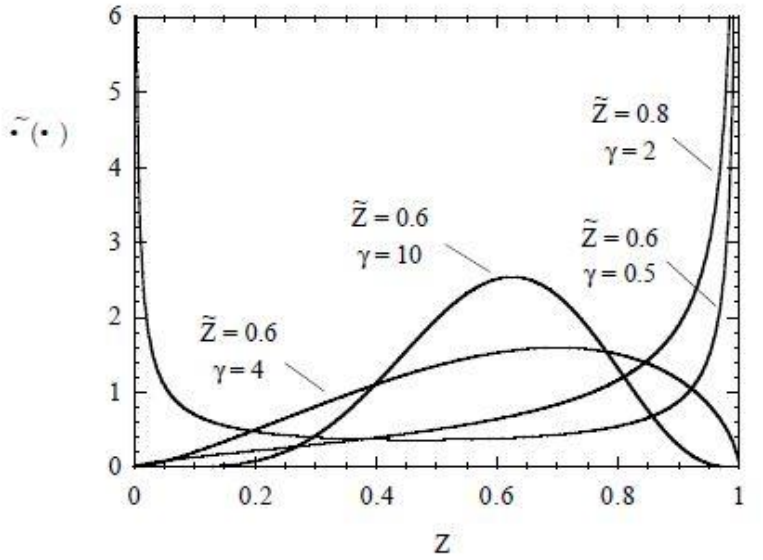

Figure 3.4: β -PDF illustration with respect to different values [42]

When combining the solution in the flamelet domain and the probability density function, we can compute the Favre-averaged mass fraction of each species, $\tilde{Y}_k$ in the physical domain as a next step. The calculation methodology is that:

$$\tilde{Y}_k(\vec{x},t) = \sum_{i=1}^{N_{cells}} \tilde{Y}_k(Z,t)\tilde{P}\,(Z;\vec{x},t)\Delta Z \tag{3.28}$$

Moreover, the temperature field is obtained by combination of new chemical composition and total enthalpy as below.

$$\tilde{Y}_k(\vec{x},t) = \sum_{i=1}^{N_{cells}} \tilde{Y}_k(Z,t)\tilde{P}\,(Z;\vec{x},t)\Delta Z \tag{3.29}$$

$$\tilde{h}_s(\vec{x},t) = \sum_{i=1}^{N_{cells}} \tilde{Y}_k(\vec{x},t)\tilde{h}_k(\vec{x},t) \tag{3.30}$$

To sum up the procedure, the chemical composition in the physical (CFD) domain is obtained according to mixture fraction and its variance for each flamelet (a marker, M_i is used for each flamelet in case of multiple flamelet analysis). Average stoichiometric scalar dissipation values are taken by each flamelet for every time-step to solve flamelet equations. Then, the temperature field is calculated by new chemical composition and total enthalpy. A representative scheme for interaction of RIF (or mRIF: Multiple Representative Interactive Flamelet) model is given (Fig. 3.5).

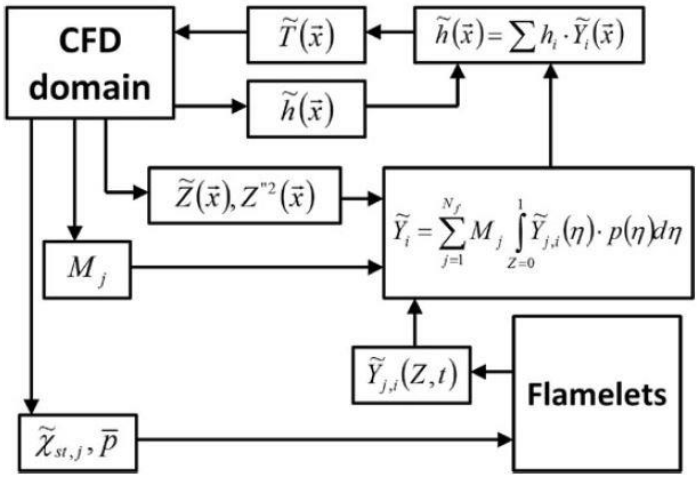

Figure 3.5: Representation of interaction for RIF model [8]

In order to decrease the computational effort, virtual species method can be adopted to RIF model. Virtual species model indicates that reduced chemical species are treated in the physical domain by considering the mass and thermodynamic properties of each chemical species in the flamelet domain.

3.2 Tabulated Chemistry

It is essential to obtain accurate models which describe the combustion phenomena within the engine as fast as possible. Since the time required to solve a simulation with direct integrated chemistry is too much particularly for industrial applications due to number of species to be used in the model, a solution is proposed to reduce CPU time in a significant way. This solution is tabulated kinetics which stores the chemical species reaction rates in a table with respect to mechanism and flame structure. Then, these stored values such as temperature, pressure are re-taken as a function of state [23, 24]. Following demands should be provided by the tabulated mechanism in order to be used in engine simulations:

- Consideration of table size due to memory restriction
- Consistency with direct integration combustion method
- Assignment of minimum number of transport equations in order to couple with the physical domain

The tabulation can be sub-divided into two categories which are internal tabulation and external tabulation. These sub-categories are examined in detail in the following sections.

3.2.1 Internal Tabulation

Tabulation is performed during the computational fluid dynamics simulation. The aim is to use more detailed chemical mechanism for better prediction of the combustion by increasing the number of species and reducing the computational effort by reutilizing the data which is requested. *ISAT, DAC* and combination of these methods which is called as *TDAC* algorithms are expressed respectively.

ISAT-In situ Adaptive Tabulation

The In situ Adaptive Tabulation, *ISAT* algorithm is used reuse computational data by storing them [7, 12]. unfeasibility of integration of tabulation into detailed kinetics due to high number of storages and operations. To do this, a linear approximation is made for query point ϕ^q during the calculation. Then, the error related to approximation is defined as the difference between exact and linearized values. If the tolerance value, ε_{tol} which is defined by user is greater than the local error value, ε, the method is described as accurate.

Tabulation of Dynamic Adaptive Chemistry, TDAC

Eventhough reduction of computational cost is achieved by *ISAT*; some adaptations can be done to develop this method. For that purpose, dynamic adaptive chemistry, *DAC* method which calculates the reduced mechanisms for local thermodynamic conditions [25] are coupled with *ISAT*; thus, the combination is called as tabulation of dynamic adaptive chemistry, *TDAC*.

DAC algorithm uses the ψ^q which is provided by *ISAT* to incorporate *ODE* set. Besides, *DAC* performs a mechanism reduction for local conditions of thermochemistry by introducing reduced set of active species, $\psi^q{}_a$, that are used by *ODE* solver. Then the calculation of the reaction mapping, $R(\psi^q)$ is performed by calculation of the reduced reaction mapping, $R(\psi^q{}_a)$ which is provided by *DAC* and used by *ISAT* [8]. Usage of TDAC method provides notable reduction for CPU cost. A schematic representation of process is shown in Fig. 3.6.

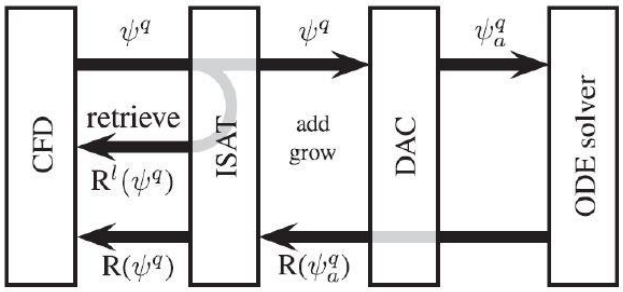

Figure 3.6: TDAC algorithm illustration [8]

3.2.2 External Tabulation

Table generation is completed before the start of simulation within this method and detailed information related to table generation and application into combustion model is given in the sections 3.2.2.1, 3.2.2.2 and 3.2.2.3 [23, 24].

Chemistry Table

A chemical mechanism and a set of initial conditions are defined for homogeneous constant-pressure reactor calculations by considering:

- Ambient pressure, p
- Initial reactor temperature, T_u
- Mixture fraction, Z and residual gas fraction, *EGR*

Although it is possible initialize temperature by assuming temperature does not depend on mixture fraction, the initialization of the temperature can be done according the values for Z = 0 and Z = 1; since, those values are specified for a spray combustion process. Those values of Z correspond to oxidizer and fuel side respectively. In addition to this, fuel heat of evaporation is used in the initialization process of the temperature. Consequently, the initial temperature of the reactor can be expressed as:

$$h(Z) = (1 - Z).h(T_{Z=0}) + Z.h(T_{Z=1}) - h_l(T_{Z=1}) \tag{3.31}$$

and

$$T_u(Z) = T\big(h(Z)\big) \tag{3.32}$$

where h_l is the vaporization heat of fuel. After computing the initial compositions, reactor calculations begin by solving chemical species equations as specified below for any determined conditions.

$$\frac{dY_i}{dt} = \dot{\omega}_i(T, p, Y_1, Y_2, \dots, Y_n) \tag{3.33}$$

The temperature of the reactor is calculated from the initial value of enthalpy. Then the operations in each time step can be split to two different branch which are progress variable, C evaluation and chemical composition evaluation with regards to virtual species method. The progress variable is defined as the heat release by combustion which is equal to enthalpy difference between initial and present value of reactor enthalpy of formation.

$$C = \sum_{i=1}^{Ns} h_{298,i} Y_i(t) - \sum_{i=1}^{Ns} h_{298,i} Y_i(0) \tag{3.34}$$

where *Ns* is the total number of chemical species. Then a normalization procedure is applied to the progress variable to store values of progress variable reaction rates and chemical composition. The normalized progress variable is shown with *c* and it is calculated as:

$$c = \frac{C - C_{min}}{C_{max} - C_{min}} \tag{3.35}$$

C_{max} and C_{min} values correspond the progress variable values at after auto-ignition condition and initial condition respectively; moreover, they are kept as a function of T_u, p, and Z in the table. As a next step, progress variable reaction rate, $\dot{c}$ is calculated by forward differencing scheme with respect to c values.

$$\dot{c} = \frac{c_{i+1} - c_i}{t_{i+1} - t_i} \tag{3.36}$$

The progress variable reaction rate, $\dot{c}$ has to be multiplied with $C_{max} - C_{min}$ to be used as a source term properly in its own transport equation. Additionally, the tabulation is done for only seven species (N_2, O_2, CO, CO_2, H_2O, H_2 and fuel) called as virtual species instead of whole chemical species in order to prevent storage of entire species and to reduce the size of table; furthermore, the mass fraction computation is done to conserve main thermochemical properties such as total number of *C, H, N, O* atoms, molecular mass, enthalpy and specific heat of the entire chemical mechanism. The calculation of virtual species and their compositions with respect to *c* is expressed below.

$$\sigma_C = \sum_{i=1}^{Ns} N_{C,i}.x_i = \sum_{k=1}^{Nv} N_{C,k}.x_{v,i} \tag{3.37}$$

$$\sigma_H = \sum_{i=1}^{Ns} N_{H,i}.x_i = \sum_{k=1}^{Nv} N_{H,k}.x_{v,i} \tag{3.38}$$

$$\sigma_O = \sum_{i=1}^{Ns} N_{O,i}.x_i = \sum_{k=1}^{Nv} N_{O,k}.x_{v,i} \tag{3.39}$$

$$\sigma_N = \sum_{i=1}^{Ns} N_{N,i}.x_i = \sum_{k=1}^{Nv} N_{N,k}.x_{v,i} \tag{3.40}$$

$$h = \sum_{i=1}^{Ns} Y_i.h_i(T) = \sum_{k=1}^{Nv} Y_{i,v}.h_k(T) \tag{3.41}$$

$$c_p = \sum_{i=1}^{Ns} Y_i.c_{p,i}(T) = \sum_{k=1}^{Nv} Y_{i,v}.c_{p,k}(T) \tag{3.42}$$

$$\sum_{k=1}^{Nv} Y_{i,v} = 1.0 \tag{3.43}$$

where σ is the total number of elements in reactor for carbon, hydrogen, oxygen and nitrogen, N_s and N_v are the total number of species in the entire chemical mechanism and for virtual species respectively, Y is the mass fraction, x is the mole fraction and N is the total number of elements in each chemical species. In addition to this, c_p is the specific heat and h is the mass specific enthalpy.

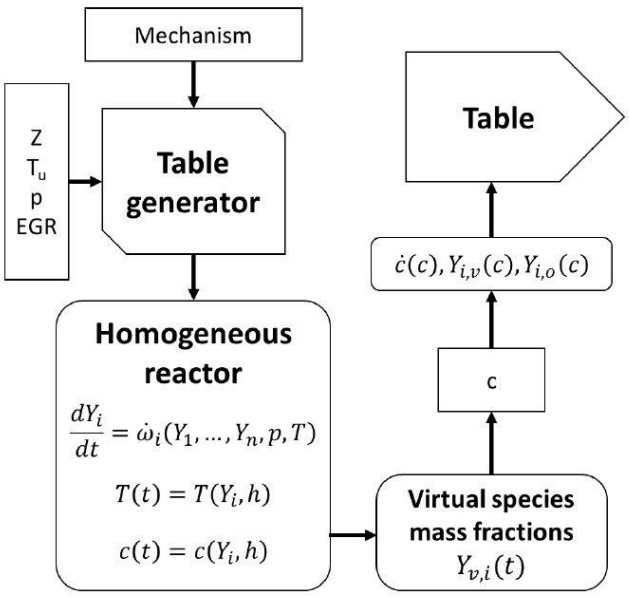

Figure 3.7: Chemistry table generation [23]

As seen in the formulas, a consistency should be between the entire chemical species and the virtual species. A summarizing figure for the chemistry table production is given by Fig. 3.7.

Governing Equations

Transport equations governing the progress variable, unburned gas temperature, enthalpy and mixture fraction are solved in the physical domain and the table is used to calculate chemical composition and the progress reaction rate. Table values at cell states are interpolated by inverse, distance weighted method. Depending on the combustion model the progress variable source term which is discussed in chemistry table section is used in the transport equation of progress variable, *C* as:

$$\frac{\partial \bar{\rho}\tilde{C}}{\partial t} + \nabla\left(\bar{\rho}\tilde{U}\tilde{C}\right) - \nabla\left(\frac{\mu}{Sc_{\tilde{z}}}\nabla\tilde{C}\right) = \rho\dot{C} \tag{3.44}$$

Additionally, an equation needs to be solved for the unburned gas enthalpy to reach the values in the table properly. Moreover, the outcome of the enthalpy is used for the gas temperature evaluation. By defining the α_t as turbulent thermal diffusivity, ρ_u as density of unburned gases, chemical composition where *C* is equal to 0 and spray evaporation terms as $T_u.\dot{Q}_s$, and its values are are not same in case of mixing line assumption or without mixing line assumption. The formula of enthalpy becomes:

$$\frac{\partial \bar{\rho}\widetilde{h_u}}{\partial t} + \nabla\left(\bar{\rho}\tilde{U}\widetilde{h_u}\right) - \nabla\left(\alpha_t\nabla\widetilde{h_u}\right) = \dot{Q}_s + \frac{\bar{\rho}}{\bar{\rho}_u}.\frac{D\bar{p}}{Dt} \tag{3.45}$$

Tabulated kinetics is performed for Representative Interactive Flamelet Model as TRIF, Well-Mixed Model as TWM. Further information related to those models is expressed in the following sections. In addition to that, Approximated Diffusion Flamelet Approach, ADF is briefly described since it is used for the validation and comparison of the baseline case defined in section 4.1.2.1 with other combustion models.

3.2.2.1 Tabulated Well-Mixed (TWM) Model

Well-Mixed approach, which does not account a relation between turbulence and chemistry, assumes that the mixture within each cell is a closed homogenous system and calculates the chemical species reaction rates by solving species and energy equations based on thermodynamic conditions such as temperature, pressure and species mass fraction and updating the mass fraction values in each computational time step. The coupling between well-mixed model and tabulated mechanism is done by solving the transport equations in the physical domain and providing the table data to the local cell vales as reported in the governing equations for externally tabulated mechanism section. The Fig. 3.8 represents the scheme of Tabulated Well-Mixed, TWM Model.

The transport equation for the mixture fraction for Tabulated Well-Mixed Model which involves the fuel evaporation is reported as:

$$\frac{\partial Z}{\partial t} + \nabla(\rho U Z) - \nabla(\mu_t \nabla Z) = \dot{S}_Z \qquad (3.46)$$

where $\dot{S}_Z$ represents the fuel evaporation. Because there are no interactions between the chemistry and turbulence in the well-mixed model, the equations described in the governing equations can be used directly by assuming:

$$\dot{C} = (C_{max} - C_{min}).\dot{c} \qquad (3.47)$$

and the transport equations are:

$$\frac{\partial \bar{\rho}\tilde{C}}{\partial t} + \nabla\left(\bar{\rho}\widetilde{U}\tilde{C}\right) - \nabla\left(\frac{\mu}{Sc_{\tilde{z}}}\nabla\tilde{C}\right) = \rho\dot{C} \qquad (3.48)$$

$$\frac{\partial \bar{\rho}\widetilde{h_u}}{\partial t} + \nabla\left(\bar{\rho}\widetilde{U}\widetilde{h_u}\right) - \nabla\left(\alpha_t \nabla\widetilde{h_u}\right) = \dot{Q}_s + \frac{\bar{\rho}}{\bar{\rho}_u}.\frac{D\bar{p}}{Dt} \qquad (3.49)$$

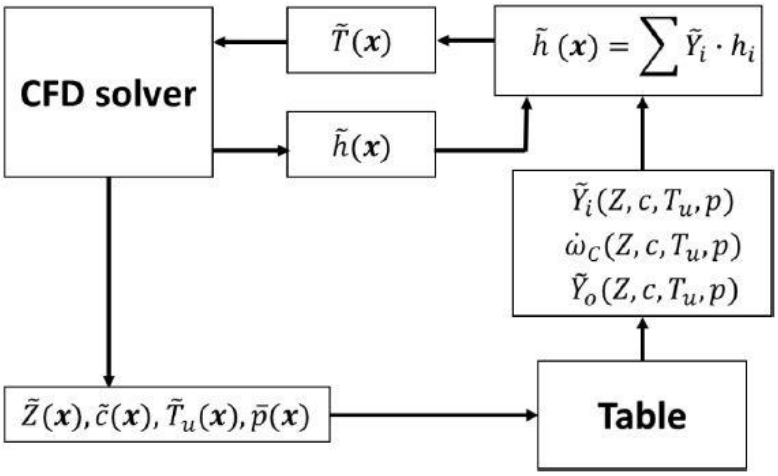

Figure 3.8: Scheme of TWM model [23]

In conclusion, although there are significant simplifications due to reduction of the dimension of the problem from $N_s + 2$ to four dimensions, similar results for well-mixed model and tabulated well-mixed model is expected. This reduction of the dimension results an effect on ignition process when progress variable is diffused to rich mixtures for a condition ϕ >3 where single stage rapid ignition and long ignition delay occurs. Therefore, reaction rates are kept zero in the region where ϕ = 3 due to prevent instantaneous ignition, and diffusion of high values of progress values back to lean or stoichiometric mixtures which leads to expected auto-ignition. However, fixing progress variable to zero value for rich mixture condition, may results some negative effects on prediction of soot formation as soot is promoted in highly rich region.

3.2.2.2 Tabulated Representative Interactive Flamelet (TRIF) Model

As mentioned in section 3.1, this approach applies laminar flamelet concept where the substantial fraction of the chemical reactions occurs in flamelets and the overall turbulent flame can be stated as ensemble of multiple laminar flamelets. Thus, mixture fraction variable, *Z* is the only parameter for all reacting scalars and *Z* depends on local air-fuel ratio for non-premixed combustion. In the CFD domain, prediction of the local chemical composition is achieved by mixture fraction variable field and the sub-grid distribution of chemical composition is characterized with a β-PDF. Multiple flamelets could be used to observe turbulence effects on the flame and to investigate flame stabilization. Injected

fuel is divided into multiple flamelets. To compute chemical composition within each cell, following formula which is obtained by flamelet marker, M_j and mixture fraction is used by defining the mass fraction as $Y_{j,i}$ and number of flamlelets as N_f where *j* represents the flamelet domain:

$$Y_i(\vec{x}) = \sum_{j=1}^{N_f} M_j \int_0^1 Y_{j,i}(\tilde{Z}) P(\tilde{Z}, \widetilde{Z''^2}) dZ \tag{3.50}$$

Then a transport equation has to solved for each flamelet marker as shown below:

$$\frac{\partial \bar{\rho} \widetilde{M_J}}{\partial t} + \frac{\partial \left(\bar{\rho} \tilde{U} \widetilde{M_J} \right)}{\partial x_i} - \frac{\partial}{\partial x_i} \left(\frac{\mu}{Sc_{\tilde{z}}} \frac{\partial \widetilde{M_J}}{\partial x_i} \right) = \dot{S_{M_J}} \tag{3.51}$$

where $\dot{S}_{M_j}$ represents the spray evaporation source term. Furthermore, flamelet equations which describe local flame structure are solved in the mixture fraction space for progress variable, *C* and enthalpy with an assumption of Lewis number is equal to one:

$$\rho \frac{\partial C}{\partial t} = \rho \frac{\chi_z}{2} \frac{\partial^2 \dot{C}}{\partial Z^2} + \dot{C} \tag{3.52}$$

$$\rho \frac{\partial h}{\partial t} = \rho \frac{\chi_z}{2} \frac{\partial^2 \dot{h}}{\partial Z^2} + \frac{dp}{dt} \tag{3.53}$$

A chemistry table is used to take data of chemical composition in the mixture fraction space in the CFD domain. This procedure is the same with TWM one which is described above. Scalar dissipation rate χ_z is used to consider mixing effects caused by turbulence and flow-field. χ_z is calculated as a function of stoichiometric mixture fraction conditions $\widehat{\chi_{st,J}}$ for every flamelet. The Fig. 3.9 represents the scheme of TRIF model.

The interaction between the physical domain and chemistry table can be seen from Fig. 3.9. Equations 3.52 and 3.53 are solved in every flamelet for each time step with the values of average stoichiometric scalar dissipation rate. Then,

chemistry table is used to compute progress variable reaction rate term by using progress variable and thermodynamic properties as input with the equation 3.52.

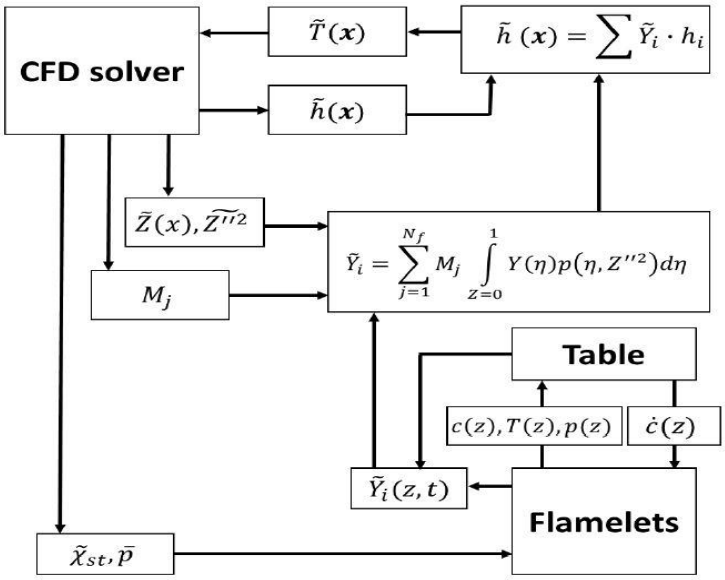

Figure 3.9: Scheme of TRIF model [24]

3.2.2.3 Approximated Diffusion Flamelet (ADF) Model

As specified in section 3.1, non-premixed combustion is modeled by flamelets in counterflow diffusion flame (DF) approach. While flamelets are defined as a one-dimensional structure in *Z*-space, temperature and species transport equations are solved for transient, mixing and source terms where these equations represent the flamelet advancement. In *Z*-space, species diffusion rate is controlled by scalar dissipation rate which is related to strain rate and contained in mixing terms. Chemical mechanism for each mixture fraction is modeled by stiff non-linear ordinary differential equations, *ODE*; furthermore, calculation of source term in transport equations is performed at each time step. Complexity of the model increases with fuel complexity since number of species and reactions can be thousands.

In this study, Tabulated Flamelet Progress Variable, TFPV library which is operated with TRIF model is presented in order to obtain unsteady diffusion flame calculations as described in ADF approach [24]. The aim of TFPV library is to describe turbulent diffusion flame by considering sub-grid mixing and pre-mixed flame propagation in addition to turbulence chemistry interaction with

reduction of computational time. A transport equation for progress variable needs to be solved in physical domain in order to achieve that. The source terms are dependent on mixture fraction and its variance, local thermodynamic properties such as pressure and temperature, and stoichiometric scalar dissipation rate.

A table is generated by the user for a specified range of thermodynamic properties and scalar dissipation rate values. Progress variable and chemical composition and can be predicted by prescribed mixture fraction values at any time step. Furthermore, TRIF data is used to consider mixture fraction variance. Then, progress variable, C and chemical composition regards to virtual species, Y_i can be estimated with respect to prescribed mixture fraction values.

$$Y_i(Z, \widetilde{Z''^2}) = \int_0^1 Y_{TRIF}(Z) P(\tilde{Z}, \widetilde{Z''^2}) \tag{3.54}$$

$$C(Z, \widetilde{Z''^2}) = \int_0^1 Y_{TRIF}(Z) P(\tilde{Z}, \widetilde{Z''^2}) \tag{3.55}$$

Finally, normalization of progress variable and estimation of progress variable reaction rate is accomplished by Equations 3.36 and 3.37 for any value of mixture fraction value and its variance. A representation of TFPV library generation is given at Fig. 3.10

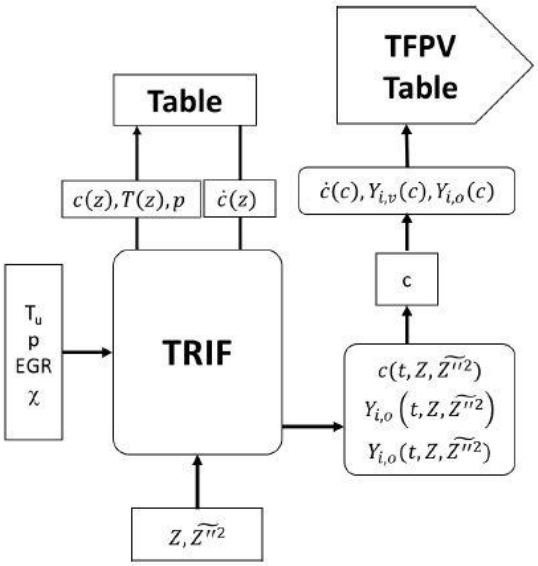

Figure 3.10: Scheme of TFPV table generation [24]

Chapter 4

Experimental and Computational Setup

This chapter includes experimental and simulation setups for described computational models in Chapter 3. Simulations are carried out for two different fuels which are n-dodecane that refers to Spray-A and dimethyl ether that refers to DME. OpenFOAM which is a free Computational Fluid Dynamics tool runs on Linux is used to perform simulations by adapting Lib-ICE applications and libraries [33] which are provided and developed by Politecnico di Milano Internal Combustion Engine group. Furthermore, experimental data for the simulations is procured by Engine Combustion Network (ECN).

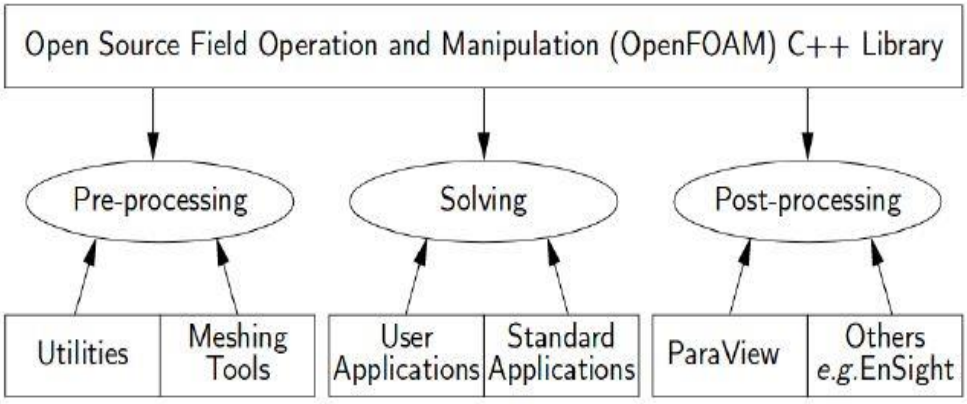

Figure 4.1: OpenFOAM process summary [26]

4.1 Spray-A Case

Experimental and computational setups of Spray-A case are explained in this section.

4.1.1 Experimental Setup Description for Spray-A

Sandia combustion vessel is used to carry out experiment of n-dodecane ($C_{12}H_{26}$) spray, Spray-A which represents the conventional diesel fuel characteristic. Combustion vessel and Spray-A case properties are reported in the following sections. All data related to experimental procedure is received form the ECN web page [19, 20, 21].

4.1.1.1 Combustion Vessel

The combustion process is proceeded in a constant vessel which has a cross-optical, cub-shaped geometry with a characteristic size of 108 mm. There are round ports at each side of the combustion chamber and their diameters are 105 mm. The Fig. 4.2 and 4.3 represent the vessel and the cross-section scheme of the combustion volume. The vessel and injector material are *AISI 4340* steel. Due to aim of heat transfer modelling at wall, a metal insert forms the right wall of the combustion chamber and the location of the injector is in metal insert, another metal insert is used to locate a fan that is used for mixing and two spark plugs at the top of combustion chamber. The other four ports are used to locate four sapphire windows to have optical access.

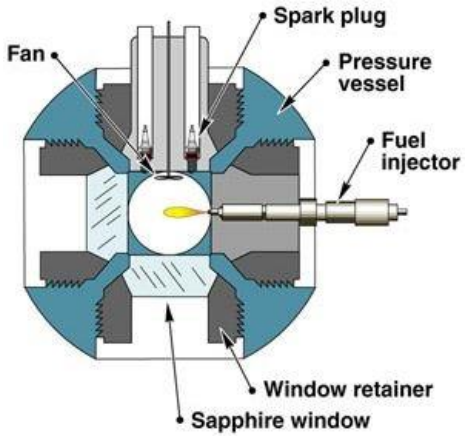

Figure 4.2: Representation of constant volume vessel [19]

The aim of the mixing fan which is located at the left corner port with a speed of 1000 rpm is to provide uniform ambient conditions when the injection starts. The fan has a 25 mm outer diameter and eight blades with 0.85 mm blade thickness; besides, the distance between the combustion vessel top wall and the bottom of the fan is 15 mm. The generation of the consistent combustion is provided by two spark plugs where the location of the gap is 16.5 mm below of the top of combustion vessel.

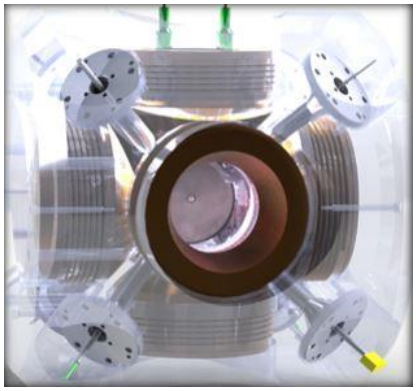

Figure 4.3: Combustion chamber [19]

The corners of the combustion chamber where there are 19.05 mm port holes, are used to locate intake and exhaust valves, or instruments like pressure transducers.

4.1.1.2 Spray-A

A figure which describes definition for nozzle orientation is given (Fig. 4.4). A cartesian coordinate system is used to locate orifice exit and the orifice location is the origin of the coordination system. θ is the orientation angle with respect to the fuel tube and injector body axis.

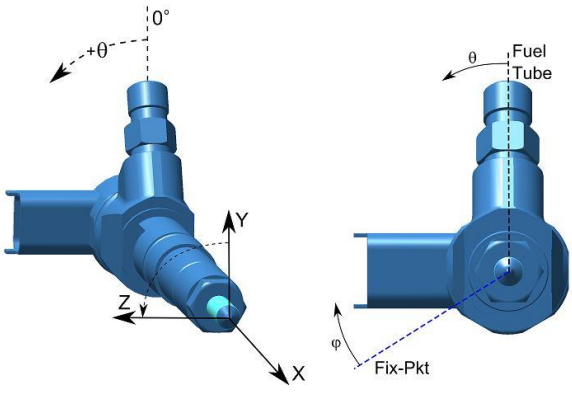

Figure 4.4: Injector orientation [21]

The specifications for the injector of Spray-A case [21] is given as a table (Tab.4.1).

Common rail fuel injector	Bosch solenoid-activated, generation 2.4
Fuel injector nominal nozzle outlet diameter	0.090
Nozzle K factor	$K = (d_{inlet} – d_{outlet})/10 = 1.5$ μm
Nozzle shaping	Smoothed by hydro-erosion
Mini-sac volume	0.2 mm^3
Discharge coefficient at 10 MPa pressure drop	C_d = 0.86 (room temperature using diesel fuel)
Number of holes	1 (single hole)
Orrifice orientation	Axial (0&deg full included angle)

Table 4.1: Injector properties

More information provided by measurements for a specific injector with 210370 serial number which is used during the simulation for comparison is given by Tab. 4.2.

Injector Serial Number	**Exit Diameter [μm]**	**θ [deg]**	**Exit offset [μm]**	**K-factor**	**Inlet radius [μm]**
210370	90.8	-90	50	1.5	23

Table 4.2: Spray-210370 additional properties

4.1.2 Simulation Model Description for Spray-A

A typical OpenFOAM case consists of three basic directories which are *0, constant* and *system* directories. All the initial and boundary conditions are hold in the 0 directories. While constant directory contains the physical model information such as mesh, thermophysical properties and combustion properties, system directory includes simulation control parameters. A simple case structure is represented in the Fig. 4.5.

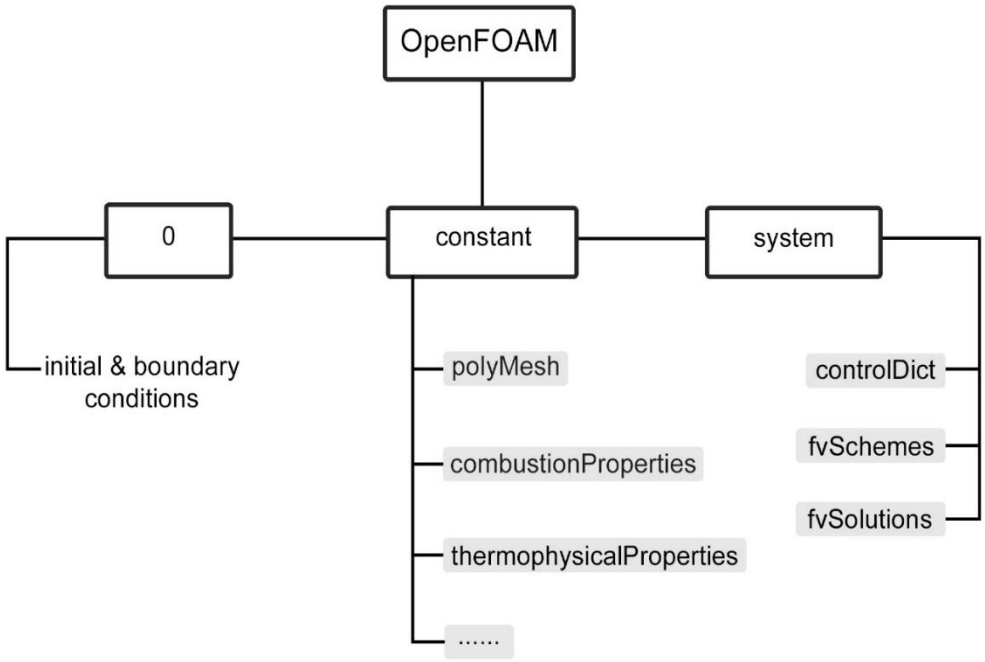

Figure 4.5: OpenFOAM case diagram

In Lib-ICE, there are two main sub-directories which are applications and src [33]. While src directory includes the libraries used by solvers, applications directory has two sub-categories named as solvers and utilities. Since the simulation is maintained at constant volume for the non-premixed combustion, the solver used for the simulations are *RIFDieselFoam* and *flameletDieselFoam*. While *RIFDieselFoam* is used for RIF and TRIF models, *flameletDieselFoam* is used for TWM case. In utilities, we have pre-processing tools for flamelet initialization such as *setTabulatedFlameletFields* for TRIF/TWM models and

setFlameletFieldsRegion for RIF model. In addition to this, utilities directory also contains post-processing tools which are *getTabulatedFlameletsData* for tabulated models and *getFlameletsData* for RIF model to obtain soot and species mass with respect to time.

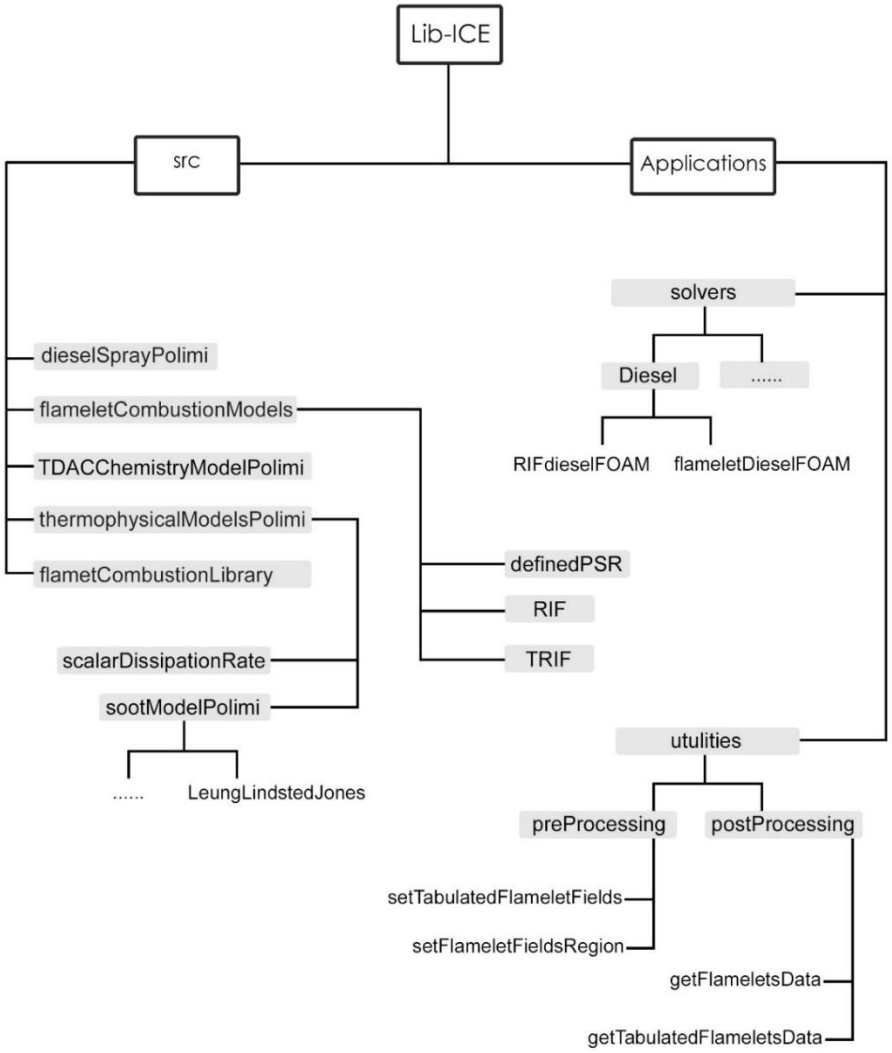

Figure 4.6: Lib-ICE diagram

Simulations are performed with RIF, TRIF, TWM and ADF models. The solvers used for different methods are described in previous section and they are introduced in Lib-ICE. Although there are certain differences between these four models, case preparation basically has the same steps because the simulations are exercised within the same conditions.

The simulated cases have three different directories which are *0*, *constant* and *system* as specified above.

0 directory

Basically, it consists of initial conditions such as pressure and temperature in addition to mass fractions of O_2, CO_2, H_2O, N_2.

constant directory

It gives physical model information used during the simulations, and important dictionaries are listed below:

- *injectorProperties*: it consists of information related to fuel injector position, fuel injection rate and other properties of the injector.
- *sprayProperties*: it includes the spray sub-model properties.
- *chemistryProperties*: it shows the method of chemistry integration.
- *combustionProperties*: it provides combustion model selection and parameters assignment.
- *thermophysicalProperties*: it gives data about thermodynamic properties of the mixture.
- *polyMesh*: this is the directory where mesh is specified.
- *RASProperties*: it provides the selection of turbulence model.

system directory

This directory includes control parameters, discretization schemes and solution method of the transport equations.

- *controlDict:* it is used to define parameters such as end time, time step of the simulation.
- *fvSchemes*: it consists of information related to discretization method.
- *fvSolution*: it defines the solution method of the transport equations.

Main procedures of the set-up by concerning significant dictionaries and initial conditions are explained in the following sections.

4.1.2.1 Initial Conditions

The simulations are carried out for several conditions that have already obtainable experimental data on the ECN web page to obtain validation of the computational models. Firstly, simulations are performed with the baseline; furthermore, models are exercised for different conditions defined by ECN to validate model is consistent to experimental data under different operating circumstances. Initial conditions for the baseline (Tab. 4.3) and other cases (Tab. 4.4 and 4.5) are given.

T [K]	p [MPa]	ρ [kg/m^3]	O_2 (volume)	CO_2 (volume)	N_2 (volume)	H_2O (volume)
900	5.98	22.8	15%	6.23%	75.15%	3.62%

Table 4.3: Initial conditions for baseline

T [K]	p [MPa]	ρ [kg/m^3]	O_2 (volume)	CO_2 (volume)	N_2 (volume)	H_2O (volume)
800	5.31	22.8	15%	6.23%	75.15%	3.62%
1000	6.62	22.8	15%	6.23%	75.15%	3.62%
1100	7.34	22.8	15%	6.23%	75.15%	3.62%

Table 4.4: Initial conditions for 15%O_2 ambient simulations

T [K]	p [MPa]	ρ [kg/m^3]	O_2 (volume)	CO_2 (volume)	N_2 (volume)	H_2O (volume)
900	5.98	22.8	13%	6.26%	77.09%	3.64%
900	6.98	22.8	21%	6.11%	69.33%	3.56%

Table 4.5: Initial conditions for 900K simulations

Within the all simulation set-ups, injection pressure and fuel temperature are kept constant at the value of 150 MPa and 373 K respectively.

```
dimensions      [0 0 0 0 0 0 0];

internalField   uniform 0.164;

boundaryField
{
    walls
    {
     type            zeroGradient;
    }
    frontWedge
    {
     type            wedge;
    }
    backWedge
    {
     type            wedge;
    }
}
```

Figure 4.7: Example of an initial condition for O_2 at baseline condition

4.1.2.2 Mesh

The chemical domain also called flamelet domain is discretized with one-dimensional mesh as reported in the Chapter 3. Mixture fraction coordinate is denoted by x-axis and gradients in other directions are ignored. Boundaries of the mesh within x direction represents the oxidizer and fuel side respectively. Oxidizer side is where x is equal to 0 and fuel side is where x is equal to one. Fig. 4.8 represents the flamelet domain.

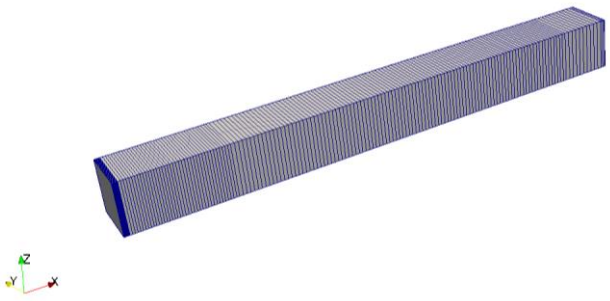

Figure 4.8: Flamelet domain representation

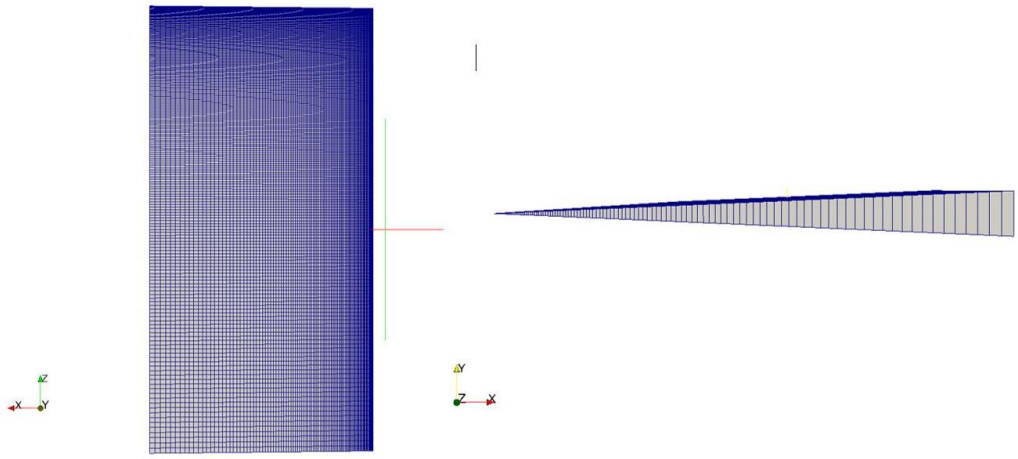

Figure 4.9: CFD domain representation

In the physical domain, the vessel is modeled as two-dimensional axisymmetric grid with a wedge angle of five degree by considering the structure of the combustion vessel. The grid has a 108 mm height and 60.9 mm radius to be consistent with the experimental conditions as a volume. Fig. 4.9 represents the used grid where a volume of 1.75071 cm^3 is produced and this volume is the 1/72 of the actual volume. The mesh type is hexahedral and total number of the cells equal to 26784 with 124 and 216 cells in radial and axial directions respectively.

```
convertToMeters 0.001;

vertices
(
    (0 0 0)
    (60.93247502 -2.660369313 0)
    (60.93247502 2.660369313 0)

    (0 0 108)
    (60.93247502 -2.660369313 108)
    (60.93247502 2.660369313 108)
);

blocks
(
    hex (0 1 2 0 3 4 5 3) (124 1 216) simpleGrading (10 1 .1)
)

edges
(
);
```

Figure 4.10: Mesh parameters used in BlockMesh dictionary

4.1.2.3 Spray and Injection Modeling

A Lagrangian model that is validated in [8], is performed in Lib-ICE in order to simulate fuel injection. Liquid spray is grouped by finite number of parcels and each parcel has equal physical properties. This modelling is called as blob injection model and used in simulations in order to describe initial conditions of the first drops at the exit of nozzle. Besides, KH-RT model [31] which is the combination of the Kelvin-Helmoltz and Rayleigh-Taylor models is used to describe primary and secondary droplet break-up regimes.

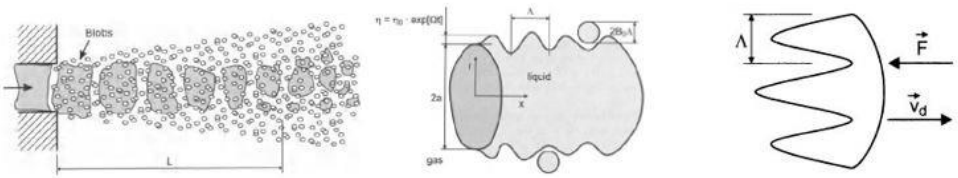

(a) (b) (c)

Figure 4.11: Blob Injection (a), Kelvin-Helmoltz (b), Rayleigh-Taylor (c) Model Representations

Injection profile which is defined in the *injectorProperties* file in constant directory of the case set-up is generated by using the CMT utility [46]. The required input variables for the rate of injection profile are back pressure, injection pressure, outlet diameter, fuel density and injection time. Although some simulations are completed for 2 ms duration due to time consideration, all simulations are performed according to 6 ms injection duration with 150 MPa injection pressure. The total amount of injected fuel corresponds to 15.7785 mg.

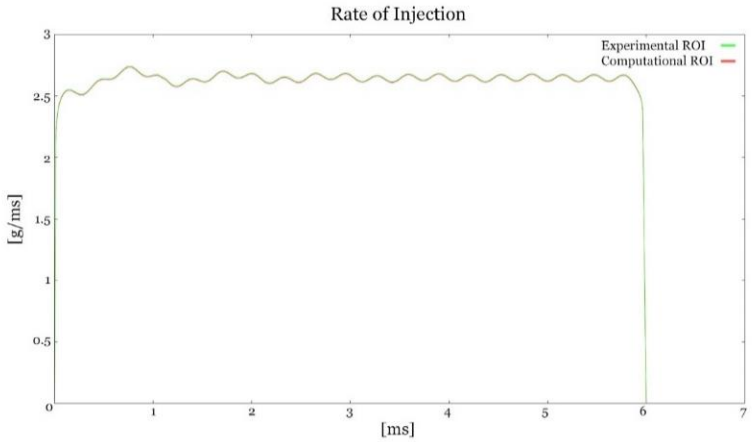

Figure 4.12: Rate of injection profile

Fig. 4.12 represents the rate of injection profile generated by CMT tool. The plot consists of two axis where y-axis is the mass per millisecond as g/ms and the x-axis is time in milliseconds.

```
    {
     injectorType        unitInjector;

     unitInjectorProps
     {
         position        (0 0 107.741e-3);
         direction       (0 0 -1);
         diameter        9.08e-5;
         Cd              0.98;
         mass            1.573479448e-05;
         nParcels        15000;
         minParcelsPerDt  1;
         temperature 373;

         X
         (
             1.0
         );

          massFlowRateProfile
         (

(    0    0    )
(    0.0000002  0.039743508    )
(    0.0000004  0.079484466    )
(    0.0000006  0.119222892    )
...
```

Figure 4.13: Example of injectorProperties directory

4.1.2.4 Chemical Mechanism

Non-premixed combustion which is known as diesel engine combustion deals with complex turbulence-chemistry interaction; thus, an appropriate chemistry should be adopted in order to predict combustion phenomena accurately. Some simplifications on the diesel fuel must be done due to large number of species, intermediate species and reactions within the combustion process. For instance, large hydrocarbon chemistry mechanism contains hundreds of species with thousands of reactions.

Two different skeletal mechanisms which are Yao and New Cai (Aachen) are adopted to simulate n-dodecane ($nC_{12}H_{26}$) fuel within the simulation. While Yao chemical mechanism which is acquired by reduction and re-optimization of detailed Lawrence Livermore National Laboratory (LLNL) includes 54 species with 269 reactions [22], New Aachen chemical mechanism contains 71 species

with 190 reactions and it is obtained by reduction and re-optimization of Narayanaswamy mechanism [37].

Although two different mechanisms are described, New Aachen chemistry mechanism is used only in RIF simulations since Yao mechanism gives more precise results compared to New Aachen one as reported in Chapter 5.

4.1.2.5 Soot

Soot modeling can be accomplished by three different models that are detailed kinetic model, empirical model or semi-empirical model. Although there are many modeling techniques to describe soot formation mechanism, it is important to minimize number of independent scalars in addition to achieve exact information for reaction steps, in order to use model in turbulent combustion. In this study, Leung Lundstedt Jones model which is based on semi-empirical method is used for soot estimation during the simulations. The soot formation mechanism which is used in our cases relies on that the major indicative for soot formation is pyrolysis intermediates, especially acetylene [36]. This soot model solves two transport equations one for mass fraction of soot and one for soot number density and soot formation mechanism is reported according to [35].

$$V\frac{\partial Y_s}{\partial x} = -\frac{\partial}{\partial x}\left(\rho V_{T,s} Y_s\right) + S_m \tag{4.1}$$

$$\frac{\partial N}{\partial x} = -\frac{\partial}{\partial x}\left(\rho V_{T,s} N\right) + S_N \tag{4.2}$$

where V is axial mass flow rate, N is the density of soot number which is defined by number of particles per unit mass of the mixture and Y_s is the soot mass fraction. While S_N which will be expressed later refers to soot nucleation and agglomeration, S_m is the source term and combined of soot nucleation, oxidation and surface growth; furthermore, they are represented by ω_n, ω_o and ω_g respectively. Thus;

$$S_m = \omega_n + \omega_g - \omega_o \tag{4.3}$$

$V_{T,s}$ represents the thermophoretic velocity of the particle and it is calculated by:

$$V_{T,s} = -\frac{\mu}{\rho T}\frac{\partial T}{\partial x} \tag{4.4}$$

where ρ is the density of the mixture and T is temperature.

To calculate soot nucleation and surface growth following chemical reactions are solved respectively:

$$C_2 \rightarrow 2C(S) + H_2 \tag{4.5}$$

$$C_2H_2 + nC(S) \rightarrow (n+2)C(S) + H_2 \tag{4.6}$$

and the reaction rates which is described by r, are expressed as:

$$r_1 = k_1(T)[C_2H_2] \tag{4.7}$$

$$r_2 = k_2(T)f(A_s)[C_2H_2] \tag{4.8}$$

$f(A_s)$ represents the function of soot surface area for unit volume and a linear dependence is used; thus, $f(A_s)$ is assumed equal to A_s. Furthermore, $k_i(T)$ is the reaction rate constant and it is expressed as:

$$k_i(T) = Aexp\left(-\frac{E}{RT}\right) \tag{4.9}$$

The coefficients for rate constant will be provided later.

Following reactions for O_2, OH and O should be considered since soot formation based on molecular oxygen and OH radical attacks with small contribution of O radicals in particular regions.

$$0.5O_2 + C(S) \rightarrow CO \tag{4.10}$$

$$OH + C(S) \rightarrow CO + H \tag{4.11}$$

$$O + C(S) \rightarrow CO \tag{4.12}$$

Following formulas represents the reaction constants of these tree reactions above.

$$r_3 = k_3(T)T^{1/2}A_s[O_2] \tag{4.13}$$

$$r_4 = \varphi_{OH}k_4(T)T^{-1/2}A_sX_{OH} \tag{4.14}$$

$$r_5 = \varphi_O k_5(T)T^{-1/2}A_sX_O \tag{4.15}$$

While φ_{OH} and φ_O are collision efficiencies attack of *OH* and *O* radicals respectively, X_{OH} and $X_O$represents mole fractions.

The source term S_N which is stated in one of the transport equations, is used to consider soot nucleation and agglomeration with the following expression:

$$S_N = \frac{2}{C_{min}}N_A r_1 - 2C_a\left(\frac{6M_{C(S)}}{\pi\rho_{C(S)}}\right)^{\frac{1}{6}}\left(\frac{6\kappa T}{\pi\rho_{C(S)}}\right)^{\frac{1}{6}}[C(S)]^{1/6}[\rho N]^{11/6} \tag{4.16}$$

while C_{min} is the carbon atoms number in the carbon particles, N_A, κ, $\rho_{C(S)}$, $[C(S)]$, $M_{C(S)}$, C_a represents the Avogadro's number, Boltzmann constant, soot density, mole concentration of soot, molar mass of soot and constant of agglomeration rate respectively.

$\mathbf{k_i}$	**A**	**E**
k_1	10000.0	41.0
k_2	3468.0	24.0
k_3	10000.0	39.0
k_4	106.0	0.0
k_5	55.4	0.0

Table 4.6: Rate constants

Soot model adaptation into simulations are made within *thermophyisicalProperties* directory. The constants are:

- *alphaTa:* nucleation exponential coefficient
- *TaOx:* O_2 oxidation exponential coefficient
- *bBeta:* surface-growth pre-exponential coefficient
- *cBeta:* agglomeration rate
- *aAlpha:* nucleation pre-exponential coefficient
- *etaColl: OH* collision efficiency
- *cOmegaOH: OH* oxidation pre-exponantial coefficient for soot formation
- *cOmegaO2:* O_2 oxidation pre-exponantial coefficient for soot formation
- *Cmin:* minimum number of carbon atoms in the particle
- *ScSoot:* dimensionless Schmidt number which is the ratio between momentum diffusivity and mass diffusivity for soot. Within soot modeling, it expresses the diffusion ratio between soot particles and mass where soot diffusion occurs in axial direction due to axial injection and mass diffusion occurs both in axial and radial direction.

Firstly, soot model implementation is done according to constant values described in [35] and constants are represented in Tab. 4.7; however, a tuning procedure for particular constants which are *cOmegaOH* and *cOmegaO2* are performed due to incorrect estimation of the soot phenomena.

***alphaTa* [K]**	21100
***TaOx* [K]**	19680
bBeta $[\sqrt{m}/s]$	6000
***cBeta* [-]**	9
***aAlpha* [1/s]**	10000
***etaColl* [-]**	0.13
***cOmegaOH* [kg.m/mol.s.**$\sqrt{K}$**]**	Variable for tuning
***cOmegaO2* [m/s]**	Variable for tuning
***Cmin* [-]**	100
***ScSoot* [-]**	0.75

Table 4.7: Soot model constants used in simulations

4.2 DME Case

DME is one of the favorable alternative fuel for diesel engines due to its similar combustion characteristic to conventional diesel fuel. Besides, DME is able to provide a zero-particle exhaust and in addition to reduction of fuel consumption, noise and NO_x formation. Consequently, combustion characteristic of the DME should be investigated in order to maximize the benefits in diesel engine applications.

Experimental and computational setup of DME (CH_3OCH_3) case is explained in this section. Since there is no experimental data provided by Sandia Engine Combustion Network for DME case, a literature research is done to obtain experimental data which are carried out in constant volume at similar conditions with Spray-A case.

All simulation conditions except for the chemical mechanism and some certain operating conditions are kept constant for DME case with respect to Spray-A case.

4.2.1 Chemical Mechanism

In order to analyze the combustion characteristic of dimethyl ether, a reduced chemical mechanism with 30 species [41] which is obtained from a detailed mechanism, is used to perform simulations for DME case, where dimethyl ether is the fuel, since performing simulations with detailed chemistry is not convenient due to high computational effort and complexity.

4.2.2 Operating Conditions

Operating conditions for DME case are determined according to [38, 39, 40] and they are shown in Tab. 4.8.

Ambient Pressure	Ambient Temperature	Injection Pressure	Injection duration	Oxygen (volume)
2.1 MPa	1084 K	40 MPa	3 ms	21%O_2
2.1 MPa	980 K	40 MPa	3 ms	21%O_2
7.04 MPa	873 K	50 MPa	6 ms	21%O_2

Table 4.8: Operating conditions for DME case

After validating the DME results with respect to experimental one, a new condition which is the baseline operating condition for n-dodecane spray, is tested and compared with Spray-A case.

Chapter 5

Experimental Validation

In this chapter, validation of two different chemical mechanisms, combustion models and soot prediction with conventional fuel n-dodecane is performed. Furthermore, DME fuel as an alternative fuel to conventional one is tested with RIF model after accuracy of the combustion model is proved.

As described in Chapter 1, heat release rate which is basically equal to lower heating value of the fuel (LHV) times combustion reaction rate, is one of the main parameters to identify diesel combustion where it is subdivided into four sub-categories. The first phase of the combustion is ignition delay where the ROHR has value around zero. This phase of the combustion also can be examined by derivation of maximum temperature of the cylinder with respect to time. The peak value of the derivation is start of the combustion process and it gives the value of ignition delay as time; furthermore, this is the methodology which is applied during the calculation of the ignition delay value. When the second phase which is premixed combustion is started, ROHR increases steeply, and it reaches to a maximum value. Then, diffusion combustion phase takes place where the heat release rate decreases and it stabilizes within a range. Finally, the late combustion occurs where heat release rate continually decreases until the value of zero; however, the last phase of the combustion is not included in the simulation since the main consideration of this study is identifying the ignition characteristic of the combustion models.

The simulation begins with start of injection which means 0 time in the plots. While the simulations are performed for 6 ms injection duration as specified in injector properties, some simulations are done until 2 ms due to time consideration.

5.1 Spray-A Validation

In this section, chemistry mechanisms, combustion models and soot formation process with Spray-A conditions are examined. Firstly, two different chemistry mechanisms are compared to each other with RIF model with regards to experimental data. Further analyses are progressed with the chemical mechanism which gives more accurate solution. Secondly, accuracy of different combustion models is examined.

Validation of the models are obtained by considering rate of heat release (ROHR), ignition delay (ID), lift off length (LOL), pressure change and maximum temperature in the combustion chamber for different operating conditions; besides, the experimental data which are provided by Sandia Laboratory are taken from ECN database [20] for comparison.

5.1.1 Chemistry Validation

Different chemical mechanisms are described in the section 4.1.2.4 for Spray-A case. The validation of the chemistry is performed with RIF combustion model. Analyses are performed initially with baseline conditions and other operating simulations are included in order to obtain reliable results. behavior of different chemistry mechanism is investigated considering the temperature and oxygen content effects separately.

The first simulation that is taken into account is baseline case where oxygen concentration is 15% and temperature is 900K. In Fig. 5.1, main results of the base case are shown (Lift-off length cannot be calculated for the RIF models due to use of single flamelet). It is clear that, although both chemical mechanisms are capable of predicting the location of the peak heat release rate value, they both overestimate the peak value. New Aachen chemical mechanism gives higher estimation of the peak value compared to Yao. After the pre-mixed combustion region, ROHR curve has to stabilize at a lower value due to diffusive combustion process. Both chemical mechanisms are well predicting the stabilization location accurate enough; however, the value of this location is overestimated by both chemical mechanism and both mechanisms show very similar trend for this region. The explanation of the higher value of the first peak and the stabilization point compared to experimental value is that while experimental data measures the apparent heat release rate which includes wall heat transfer, computational model calculates heat release rate without including heat transfer from the wall.

The average combustion vessel pressure with respect to time is directly related to combustion and it has similar trends for both chemical; besides, they both estimate the values higher than the experimental one. Maximum temperatures within the cylinder for both mechanisms are also plotted. Although there is no direct comparison for this plot, it is used to evaluate ignition delay value for the combustion process and it will be mentioned at the end of this section. Vapor penetration which is described as the maximum axial distance from injector where mixture fraction value equals to 10^{-3}, is observed. The trend of vapor penetration is well captured by both mechanisms, and the value of experimental output lies between two chemical mechanism. Experimental vapor penetration with respect to time vanishes earlier since measurement are obtained until that time value. As a note, only rate of heat release and ignition delay plots are considered for further comparisons; besides, only computational data are plotted for some outputs due to lack of experimental data for particular operating conditions.

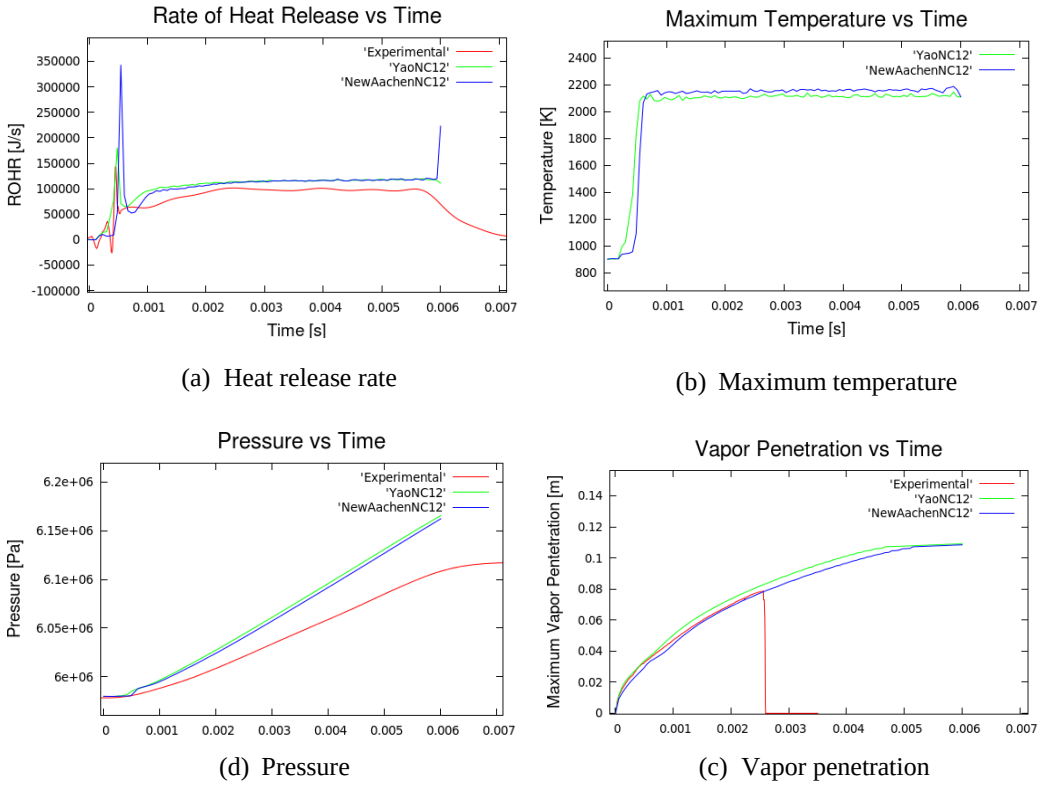

(a) Heat release rate

(b) Maximum temperature

(d) Pressure

(c) Vapor penetration

Figure 5.1: Chemical mechanism comparison with RIF model at 900K and 15%O_2 ambient condition

After obtaining the first results with the base case, effect of oxygen concentration is taken into account at same temperature value. The simulation conditions which are 13%, 15% and 21% oxygen concentration at 900K temperature are expressed in section 4.1.2.1. Fig. 5.2 shows different characteristic of ROHR plot according the different oxygen concentration. When the oxygen concentration increases, the peak value of the rate of heat release value increases and when the oxygen concentration decreases, peak value decreases. While the Yao mechanism underestimates the peak value for higher oxygen ration and overestimates it for the lower oxygen concentration, New Aachen chemistry overestimate the maximum value for all conditions. Furthermore, Yao mechanism gives more precise result in terms of heat release rate compared to New Aachen. In addition to heat release rate, ignition delay is analyzed. It has a decreasing trend from higher concentration to lower concentration due to reduction of mixing time with higher oxygen content. While New Aachen gives more accurate result in 13% oxygen concentration, Yao mechanism have more reliable results for 15% and 21% oxygen concentration.

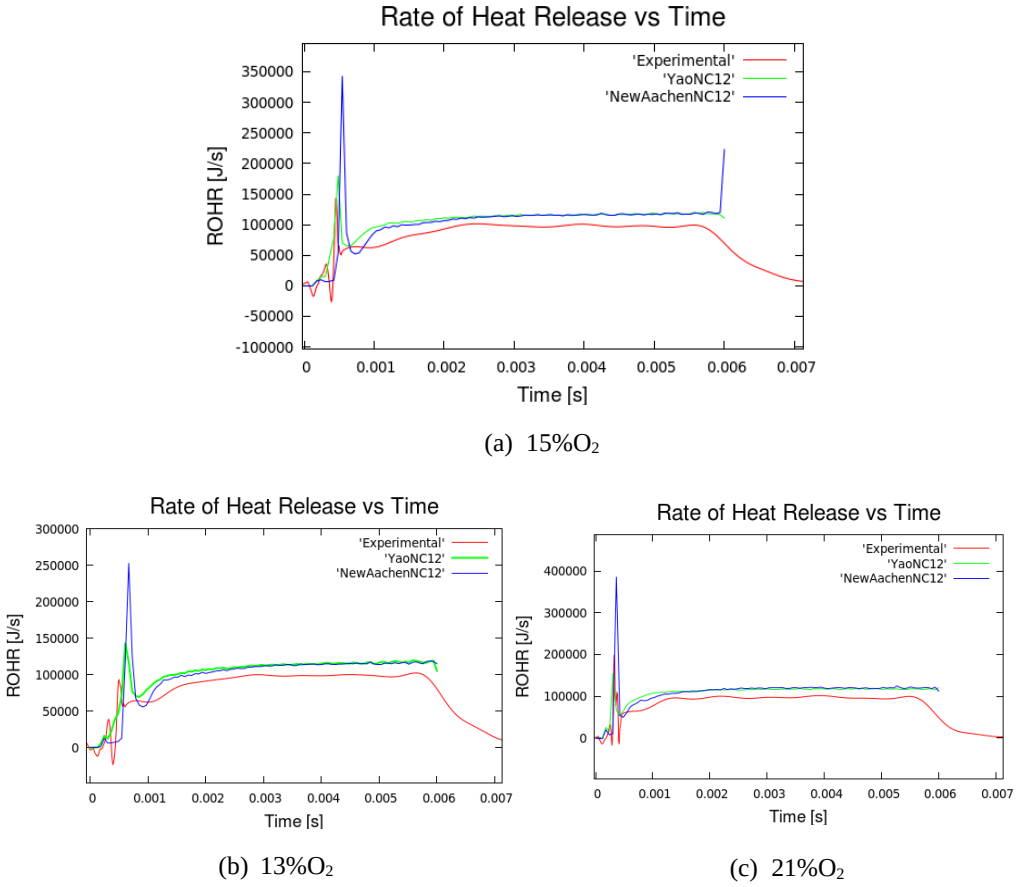

(a) 15%O_2

(b) 13%O_2 (c) 21%O_2

Figure 5.2: Comparison of chemical mechanism with RIF model at 900K with different oxygen concentrations

Finally, the effect of temperature is investigated by keeping the oxygen concentration at constant value and then varying the temperature. The conditions are reported in the section 4.1.2.1 as well. The simulations are ended at 2 milli seconds since that time is sufficient to characterize combustion. As reported the Fig. 5.3, it is obvious that increasing the temperature decreases the location of peak ROHR value and also decreases the value of the maximum value. The logic behind this, increasing the initial temperature reduces the ignition delay since the vessel is in more desirable condition; however, this condition affects the production of heat inversely since there is shorter time for mixing of air and fuel at higher temperatures for combustible mixture.

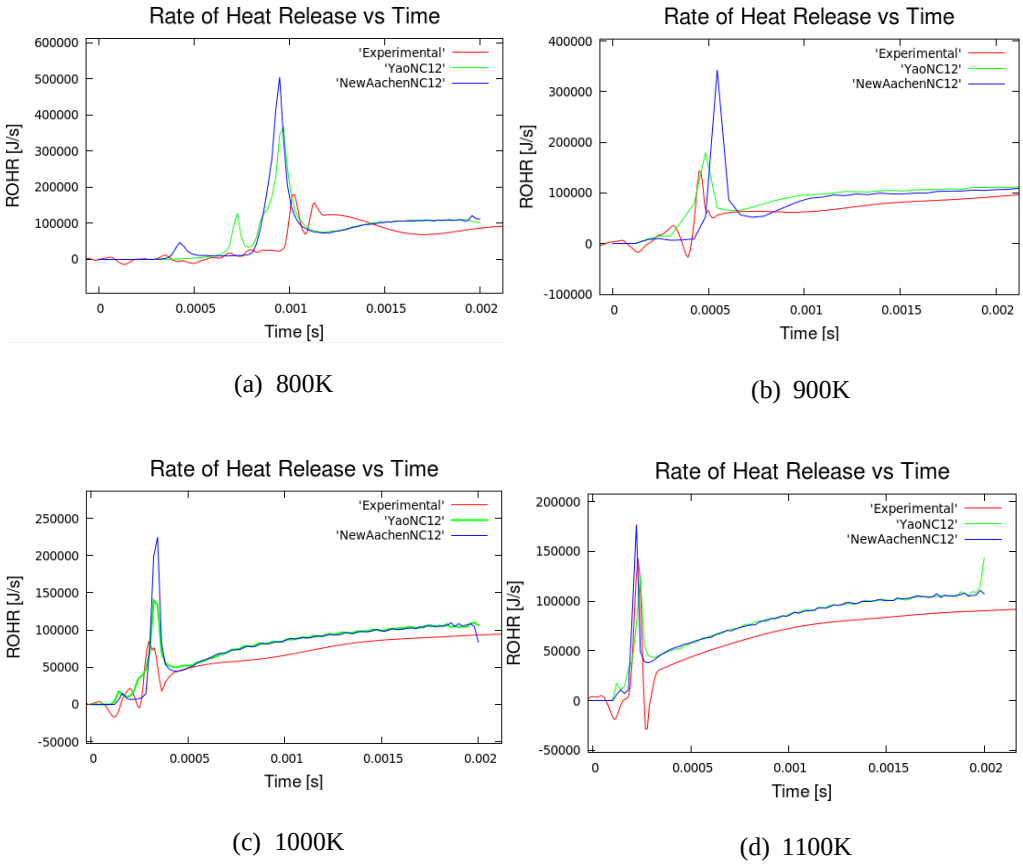

(a) 800K

(b) 900K

(c) 1000K

(d) 1100K

Figure 5.3: Chemical mechanism comparison at 15%O_2 ambient conditions

In Fig. 5.4 the effect of the oxygen concentration and temperature on heat release rate is represented by using the experimental data in order to realize the behavior of the ROHR curve more precisely.

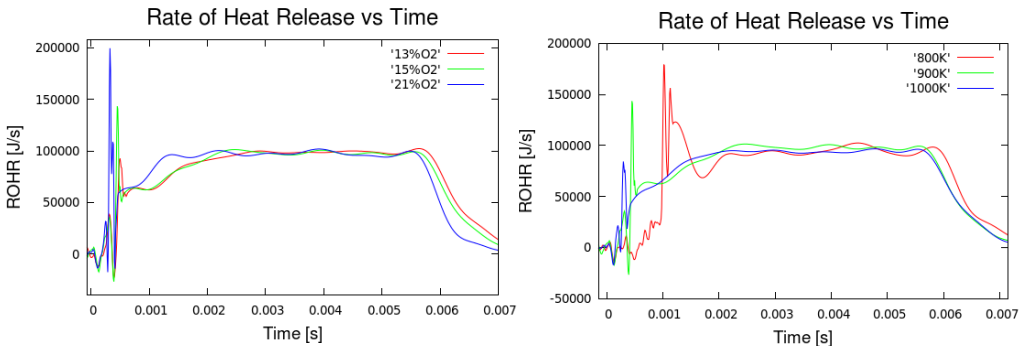

(a) (b)

Figure 5.4: Effect of oxygen concentration at 900K ambient conditions (a) and effect of temperature at 15%O2 ambient conditions (b) on heat release rate

To conclude, even though both chemistry mechanisms give precise results with respect to experimental data, Yao chemical mechanism has more sufficient values by means of ignition delay which is calculated by obtaining peak value of the derivation of maximum temperature in the combustion chamber with respect to time. Thus, further simulations for combustion model validations are performed by using YaoNC12 chemistry.

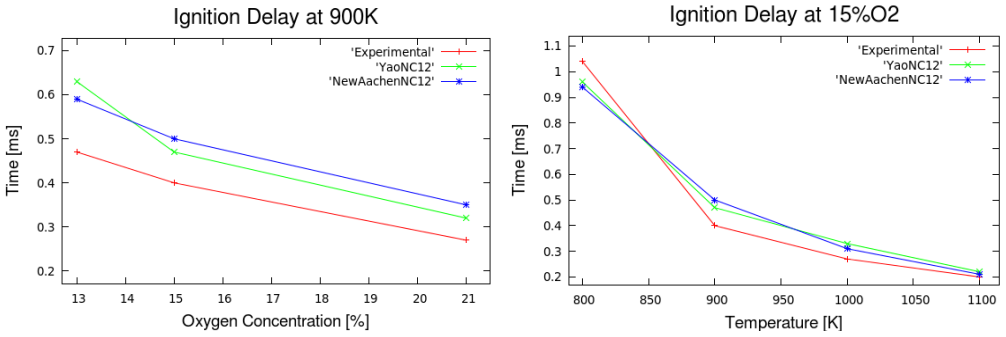

(a) (b)

Figure 5.5: Ignition delay at 900K (a) and 15%O2 (b) ambient conditions

	13%O2	**15%O2**	**21%O2**
YaoNC12	0.63	0.47	0.32
NewAachenNC12	0.59	0.50	0.35
Experimental	0.47	0.40	0.27

Table 5.1: Ignition delay values [ms] of YaoNC12, NewAachenNC12 and experimental results at 900K ambient conditions

	800K	**900K**	**1000K**	**1100K**
YaoNC12	0.96	0.47	0.33	0.23
NewAachenNC12	0.94	0.50	0.31	0.21
Experimental	1.04	0.40	0.27	0.20

Table 5.2: Ignition delay values [ms] of YaoNC12, NewAachenNC12 and experimental results at 15%O_2 ambient conditions

5.1.2 Combustion Model Validation

This section mainly focuses on comparison of RIF and TWM models. In addition to that, TRIF model included for different temperature conditions and ADF model is only accounted for baseline condition to obtain overall comparison within all combustion models. Initially, comparison for Tabulated Well-Mixed Model, TWM Model and Representative Interactive Flamelet, RIF Model are performed under different temperature and oxygen concentration conditions as specified in section 4.1.2.1, then the simulations for 800 K and 1000 K conditions are performed by TRIF model. Finally baseline simulation is extended for the all combustion models which are specified in Chapter 3, to obtain overall comparisons of the models with respect to each other.

Rate of heat release and the maximum temperature in the constant volume during the combustion processes are the primary parameters to investigate model behaviors under different situations. Ignition delay is calculated by derivation of the maximum temperature with respect to time as described in section 5.1.1.

5.1.2.1 Investigation of RIF and TWM Models

Two different combustion models which are RIF and TWM are investigated in this section. In addition to tabulated chemistry, the main difference between the RIF and TWM model is that RIF model regards turbulence chemistry interactions while TWM model do not. More detailed description for the combustion models are provided in Chapter 3.

Primarily, the base case is considered; furthermore, the simulations under different operating conditions are performed in order to consider behavior of models with respect to temperature and oxygen content variation.

Fig. 5.6 represents the main outputs of the combustion process within the constant volume vessel with respect to time in 900K and 15%O_2 condition. As seen from the plots, pressure evolution within the constant vessel is slightly higher for TWM model compared to RIF model although they both yield in satisfactory results with respect to experimental values. Vapor penetration of the TWM model is predicted as between RIF model and experimental data. More detailed analyses are performed with respect to heat release and maximum temperature curve since they provide sufficient information to understand the combustion process' behavior. It can be said that both combustion models estimate the location of the maximum heat release rate value differently than the experimental value. While TWM model underestimates both the location and the value of peak point, RIF model overestimates both of the peak point location and peak point value. After the pre-mixed combustion phase, TWM curve stabilizes earlier with respect to RIF model and experiment. Ignition delay affects the ROHR curve characteristic. Hence, TWM model has lower ignition delay. It is normal to expect lower peak value of the heat release rate curve since there is less time for mixing process which results auto-ignition. Furthermore, the main reason of having different rate of heat release curve is that transition from auto ignition region to diffusion combustion region is different due to turbulence chemistry interaction consideration of the combustion models as described in Chapter 3. Higher value of the heat release rate curve for both combustion models after auto-ignition phase has the same reason with discussed in section 5.1.1. Maximum temperature curve shows a steeper increment and higher stabilization value for TWM model. Since TWM model has higher burning rate, it is expectable that TWM model has higher maximum temperature. In addition to this, it can be observed that, TWM model has the maximum slope point, which gives an information related to ignition delay, earlier than the RIF model. Consequently, TWM model has lower ignition delay and lower peak value for rate of heat release compared to RIF model.

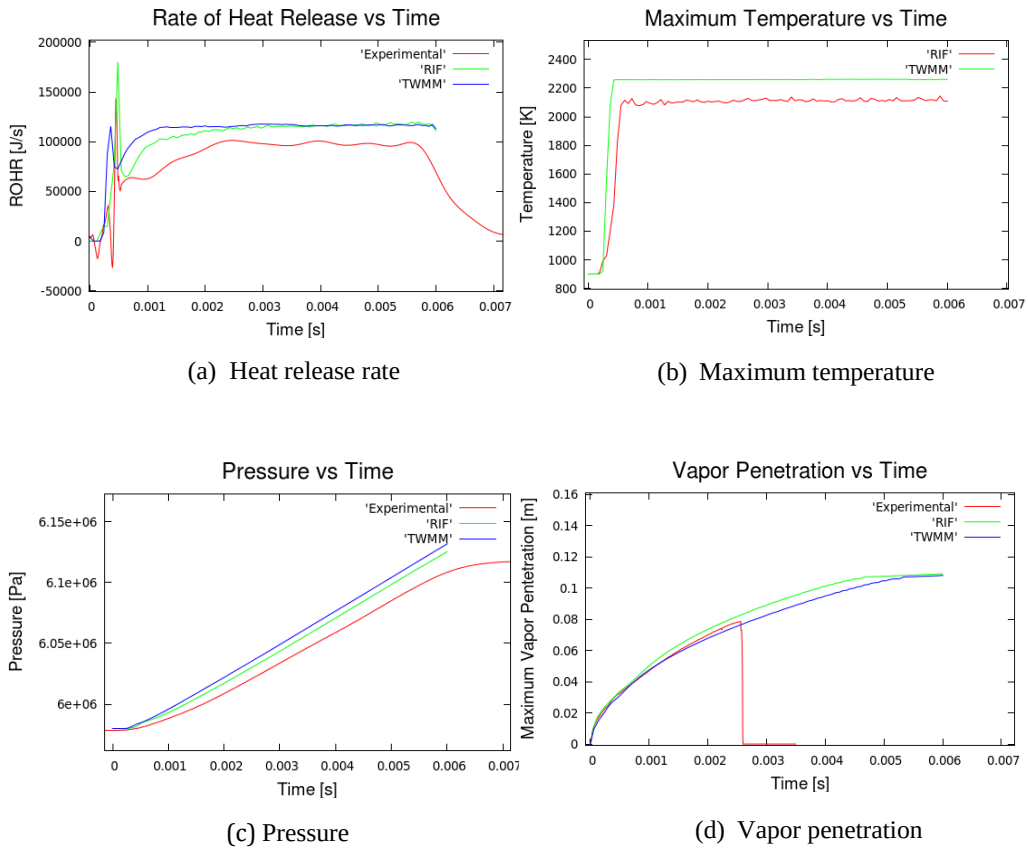

(a) Heat release rate

(b) Maximum temperature

(c) Pressure

(d) Vapor penetration

Figure 5.6: Comparison of RIF and TWM models at 900K and 15%O_2 ambient condition

When the baseline simulation is concluded, other simulation conditions are performed in order to understand the capability and accuracy of the combustion models under different operating circumstances. To do this, different oxygen concentration under same temperature value and different temperature values having same oxygen concentration conditions are taken into consideration as mentioned previously in section 4.1.2.1. Firstly, different oxygen concentration will be considered to analyze how models react for different oxygen content. Then, temperature effect is going to be detailed to see behavior of the models under different initial temperature conditions.

The trend for the rate of heat release curve for different oxygen content is given section 5.1.1 experimentally. By considering that, the results for different oxygen concentration for RIF and TWM models are shown in Fig. 5.7.

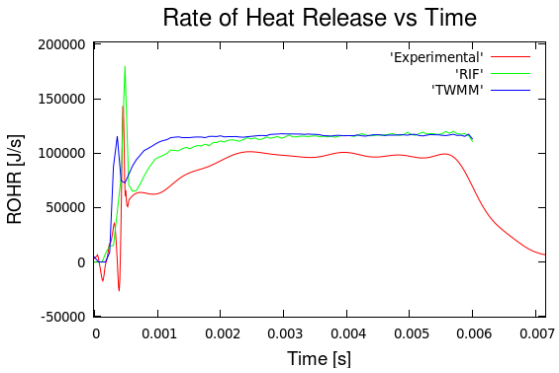

(a) 15%O_2

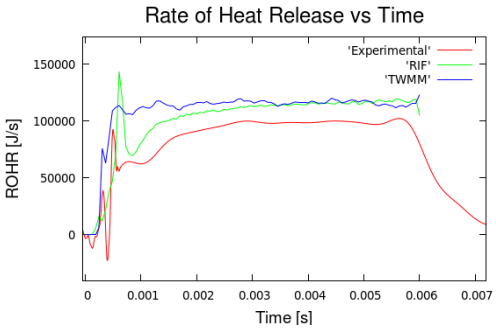

(c) 13%O_2

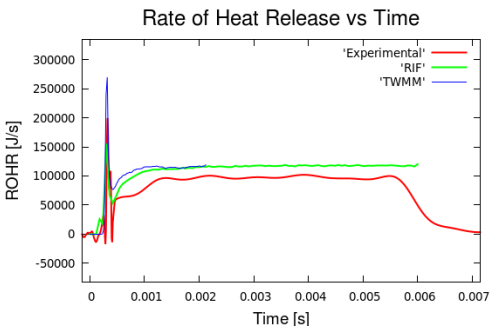

(b) 21%O_2

Figure 5.7: Heat release rate of RIF and TWM models at 900K ambient conditions

When the oxygen content increases, the maximum value of the heat release rate increases for both combustion models; besides, RIF model is able to catch peak point location better than TWM model. While TWM model underestimates the peak heat release rate value under 13% and 15% oxygen concentration conditions, and overestimates it under 21% oxygen concentration condition, RIF model overestimate the peak value at 13% and 15% oxygen concentration conditions and underestimate it at 21%oxygen concentration condition. Although RIF and TWM models have similar value for ROHR where diffusion combustion occurs, the transition from auto-ignition to diffusive combustion is different. TWM simulations have faster transition compared to RIF ones. If the ignition

delay is considered, TWM model underestimates at low oxygen concentration; however, it gives higher values under high oxygen concentration conditions compared to experimental data. In addition to these, higher value of ignition delay is always obtained by RIF model. RIF and TWM models have very close values for 21% oxygen concentration condition. Ignition delay results under different oxygen concentrations are given in Fig. 5.8.

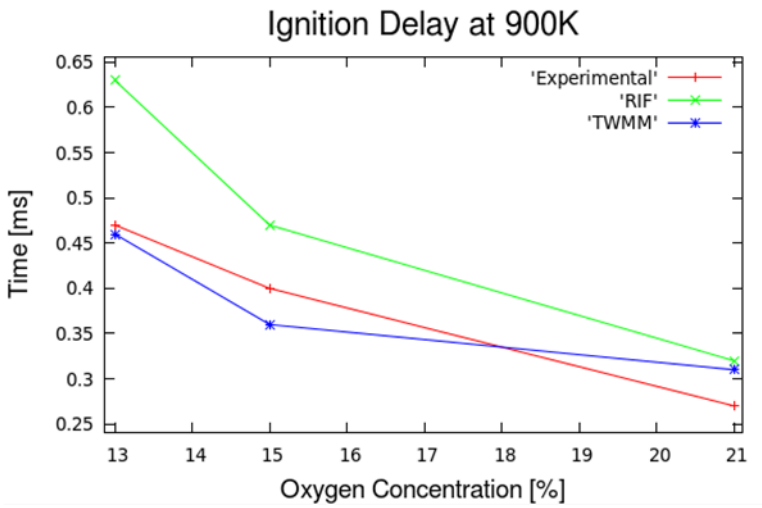

Figure 5.8: Ignition delay comparison of RIF and TWM models at 900K ambient conditions

The behavior of the combustion models under different temperature conditions with constant oxygen concentration is exercised by considering the actual trend of combustion process specified in section 5.1.1. In general, it can be pointed out that while ignition delay and maximum value of heat release rate decrease, the maximum value of the heat release rate increases at higher temperature conditions.

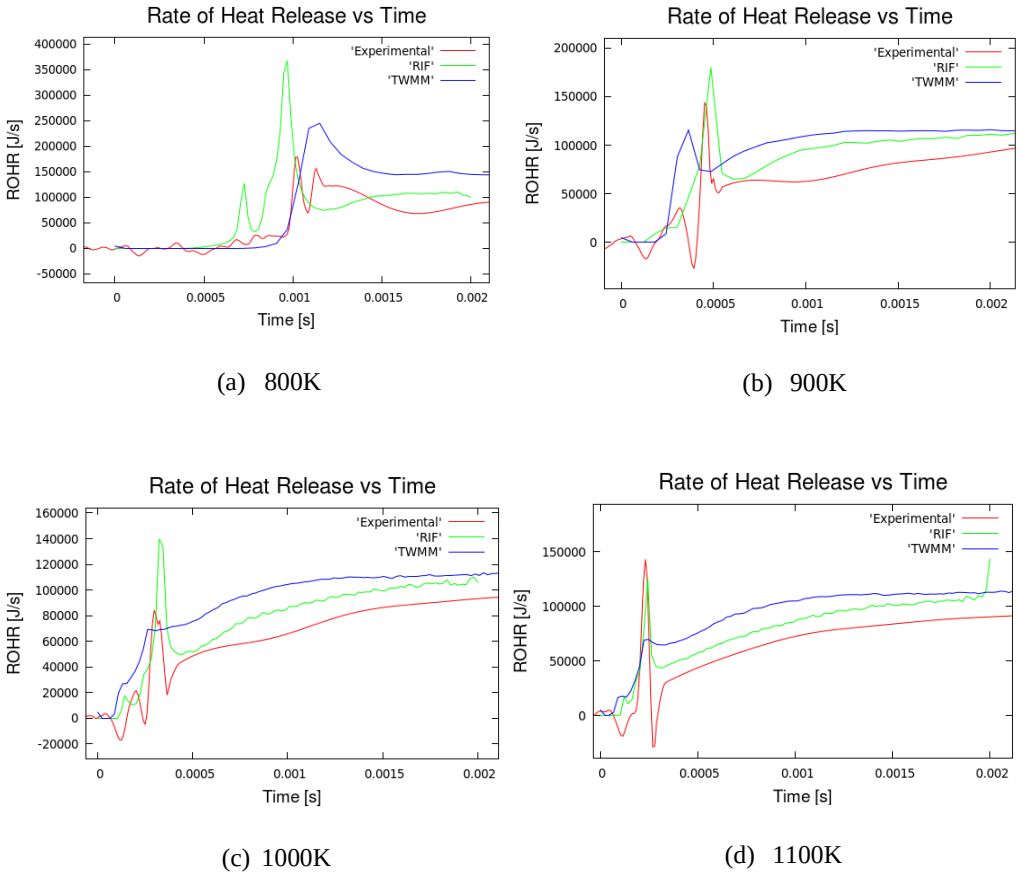

Figure 5.9: Heat release rate of RIF and TWM models at 15%O_2 ambient conditions

Fig. 5.9 represents the comparison of combustion models under different temperature conditions with respect to experimantal data. TWM model gives more accurate results with regards to location of maximum heat release rate point. RIF model predicts the ROHR curve more precisely; however, it has poor result at 800K condition. TWM model underestimate the peak value for heat release rate except for the 800K condition. As seen at different oxygen content plots, TWM model still have faster transition from auto-ignition to diffusive combustion region. Ignition delay values and possible trends for two different combustion models are given by taking into account the experimantal data (Fig. 5.10). TWM model gives more accurate results in all conditions in terms of ignition delay; nevertheless, it underestimates the value at low temperature and ovestimate the value at higher temperatures.

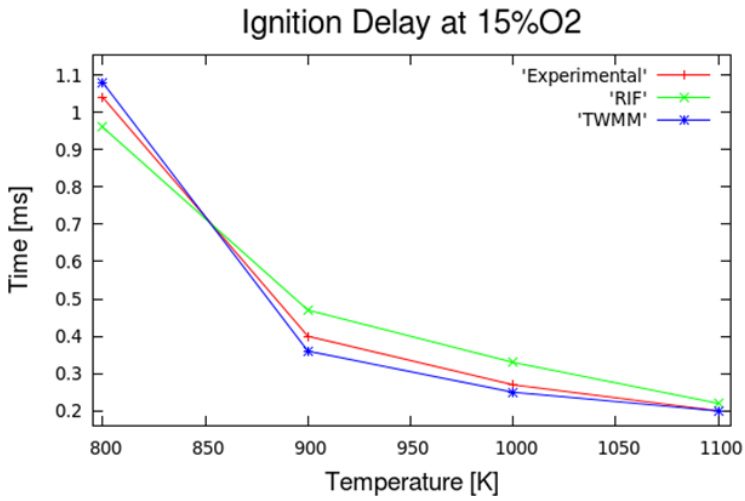

Figure 5.10: Ignition delay comparison of RIF and TWM models at 15%O_2 ambient conditions

Lift-off length (LOL) of the TWM model with respect to experimental values are plotted in Fig. 5.11. Lift of length is only plotted by TWM model since simulation with RIF and TRIF models are performed only with one flamelet which means there is no flame lift-off.

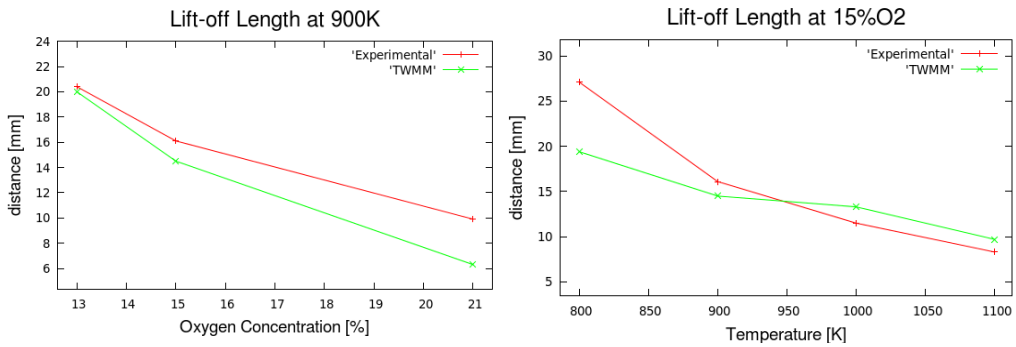

Figure 5.11: Lift-off length of TWM model at 900K and 15%O_2 ambient conditions

It is noticeable that TWM model results similar approximation under 900K and 13%O_2 condition. When the oxygen concentration is increased, the difference between computational and experimental data is expanded; moreover, TWM model always underestimate the LOL value under 900K conditions. In addition

to that, TWM model seems to catch LOL length in a better way at high temperature level compared low temperature one. While it gives a lower prediction until approximately 950K level, it results slightly higher estimation of LOL beyond that temperature level.

In conclusion, RIF model has more realistic curve in terms of peak value of rate of heat release and transition from pre-mixed combustion to diffusive combustion region. However, TWM model is more capable of determination of ignition delay value. The ignition delay values for all simulated conditions are summarized in the Tab. 5.3 and 5.4.

	13%O2	**15%O2**	**21%O2**
RIF	0.63ms	0.47ms	0.32ms
TWMM	0.46ms	0.36ms	0.31ms
Experimental	0.47ms	0.40ms	0.27ms

Table 5.3: Ignition delay values [ms] of RIF and TWM models with respect to experimental results at 900K ambient conditions

	800K	**900K**	**1000K**	**1100K**
RIF	0.96ms	0.47ms	0.33ms	0.23ms
TWMM	1.08ms	0.36ms	0.25ms	0.21ms
Experimental	1.04ms	0.40ms	0.27ms	0.20ms

Table 5.4: Ignition delay values [ms] of RIF and TWM models with respect to experimental results at 15%O_2 ambient conditions

5.1.2.2 Investigation of TRIF Model

Behavior of TRIF model under different operating conditions is examined with respect to RIF model and experimental data. Simulations for both combustion models are carried out with only single flamlelets; thus, stabilization of flame occurs at nozzle exit after start of ignition without lift-off. Comparison of the models is started with baseline condition and it is extended to different temperature conditions in order to evaluate effect of temperature on prediction under constant value of oxygen concentration.

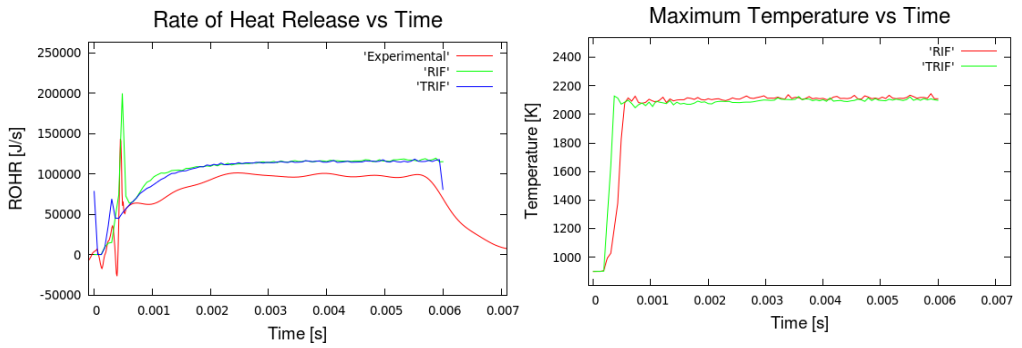

(a) (b)

Figure 5.12: Heat release rate (a) and maximum temperature (b) comparison of RIF and TRIF models at 900K and 15%O_2 ambient condition

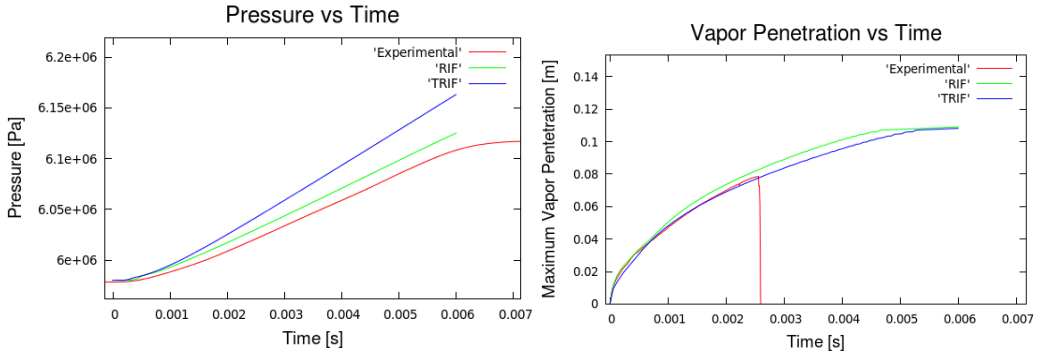

(a) (b)

Figure 5.13: Pressure (a) and vapor penetration (b) comparison of RIF and TRIF models at 900K and 15%O_2 ambient condition

Fig. 5.12 and 5.13 illustrate the heat release rate, maximum temperature, pressure and vapor penetration results with respect to time in 900K and 15%Oxygen condition. While TRIF model predicts a higher vessel pressure, RIF model remains between TRIF and experimental values. In addition to that, vapor penetration of both models represents similar curve. As seen from the figures, ignition of TRIF model starts earlier and the peak value of the heat release rate is smaller compared to RIF model. After the pre-mixed combustion region, both

models estimate behavior of mixing controlled combustion phase similarly. TRIF model reaches the maximum temperature value faster than RIF model.

After the baseline condition, behavior of the models is analyzed at different temperatures. At lower temperature level the ignition delay of the both models decrease; however, TRIF model estimates a lower value compared to RIF model. Fig. 5.14 represents the behavior of models at 800K operating condition. While TRIF model underestimates the location and value maximum heat release rate point, RIF model overestimates both location and the value. Furthermore, stabilization of heat release curve occurs earlier with respect to RIF model.

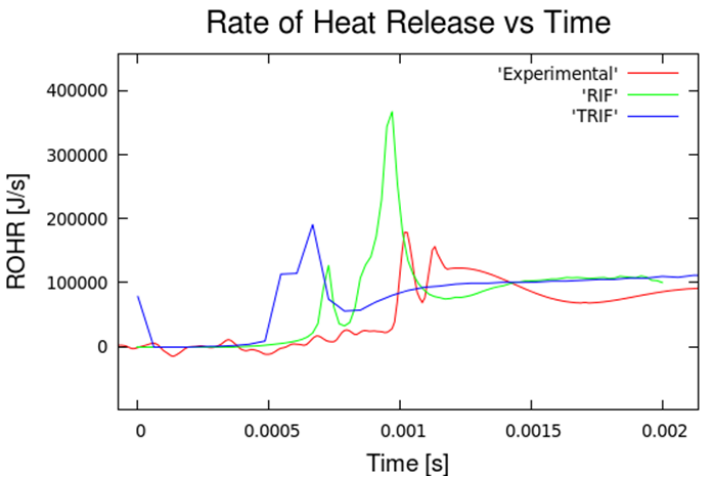

Figure 5.14: Heat release rate of RIF and TRIF models at 800K 15%O_2 ambient condition

Results of simulations which are conducted at higher temperature level are given in Fig. 5.15. It is clear that TRIF model predicts the heat release rate's maximum value and its location at lower point while RIF model is good to predict location of maximum value. The maximum temperature curve for both models seem more identical under high temperature condition; nevertheless, TRIF model still reaches maximum value faster than RIF model.

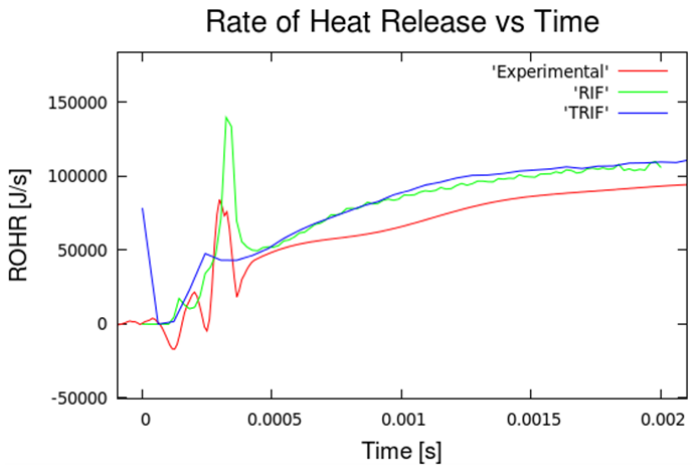

Figure 5.15: Heat release rate of RIF and TRIF models at 1000K 15%O_2 ambient condition

TRIF model always underestimates the timing where heat release rate reaches maximum point and the value of heat release rate as well compared to RIF model. Both models have similar characteristic behavior for transition from auto-ignition region to diffusive combustion region. Tab. 5.5 shows the ignition delay value of TRIF model with respect to experimental ones under different operating conditions.

	800K	**900K**	**1000K**
RIF	0.96	0.47	0.33
TRIF	0.66	0.32	0.26
Experimental	1.04	0.40	0.27

Table 5.5: Ignition delay values [ms] of RIF, TRIF models and experimental results

To conclude, TWM model is also included to make final consideration for TRIF model. Fig. 5.16 represents the ignition delay of RIF, TRIF and TWM models with respect to temperature. While TRIF model always results in lower prediction of ignition delay at all operating conditions, all combustion models which are compared until now give precise results at 1000K. In general, TWM model has

higher ability to catch ignition delay and its trend under constant oxygen concentration and different temperature situations with respect to other models.

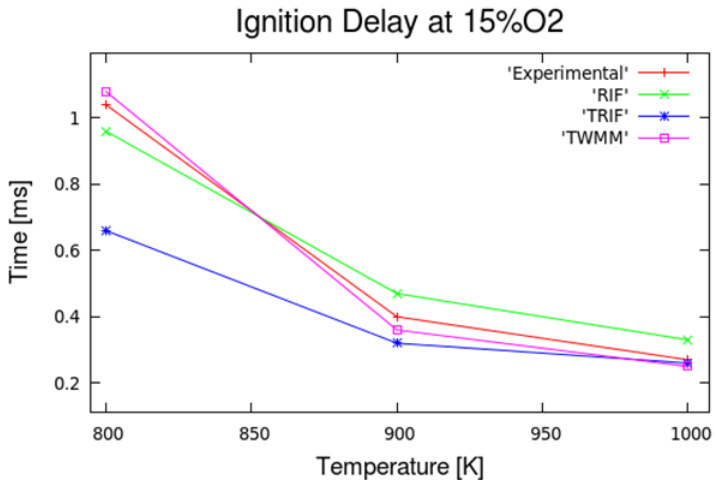

Figure 5.16: Ignition delay comparison of RIF, RIF and TWM models with respect to experimental results

5.1.2.3 Extension of Baseline Results

The base case is compared with all combustion models defined in this chapter in order to understand the behavior and the accuracy of the models. According to Fig. 5.17, location of the peak value of heat release rate and the value of maximum point are estimated differently by all models. While RIF model has the highest estimation of the maximum ROHR value, TRIF model gives the lowest estimation. TWM model and ADF model estimates the peak value location similarly; however, the maximum value is higher for TWM model. Quasi steady-state region of the heat release rate profile where diffusion combustion takes place are practiced separately for all combustion models. Shorter time is observed for TWM model since there is no turbulence and chemistry interaction considered within this model and it affects the transition from auto-ignition to mixing controlled combustion phase. In addition to this, overestimation of heat release which represents higher burning rate is occurred for TWM model due to same reason. If location of the maximum heat release rate value is not considered, TRIF and RIF models have similar characteristics for ROHR stabilization. Both RIF and TRIF models take higher duration to establish stabilization compared to TWM model due to turbulence-chemistry interactions. The time which is required for ROHR curve stabilization is the highest for ADF model.

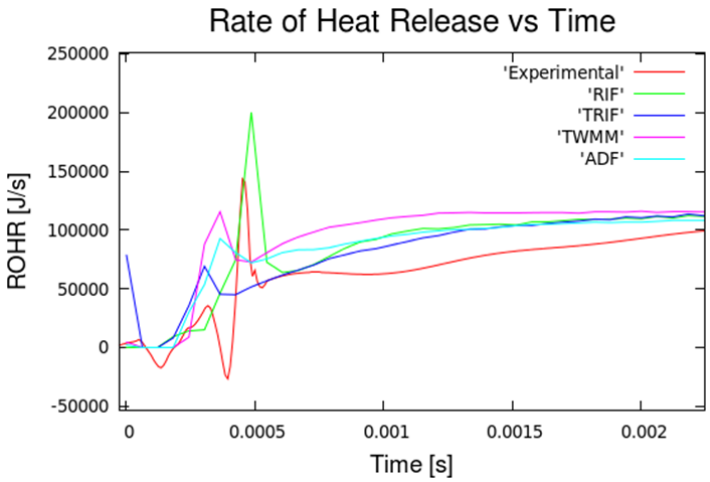

Figure 5.17: Heat release rate of RIF, TRIF, TWM, ADF models and experimental results at 900K and 15%O_2 ambient condition

Fig. 5.18 represents the maximum temperature of the constant volume vessel for all combustion models in baseline condition. As seen from the plotted data, TWM model overestimate value of the maximum temperature due to elimination of turbulence chemistry interaction which results very thin flame structure and higher burning rate estimation. RIF and TRIF model predict the maximum temperature precisely with respect to each other; however, the location where maximum temperature is reached, are not same due to different ignition delay values. ADF model underestimates the maximum temperature until stabilization point of heat release rate.

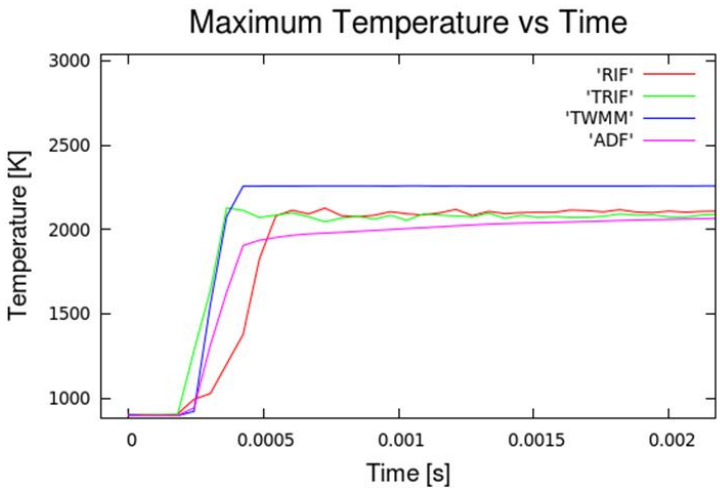

Figure 5.18: Maximum temperature of RIF, TRIF, TWM and ADF models at 900K and 15%O_2 ambient condition

Ignition delay is investigated in the same methodology as mentioned in 5.1.1 and it is represented in Fig. 5.19.

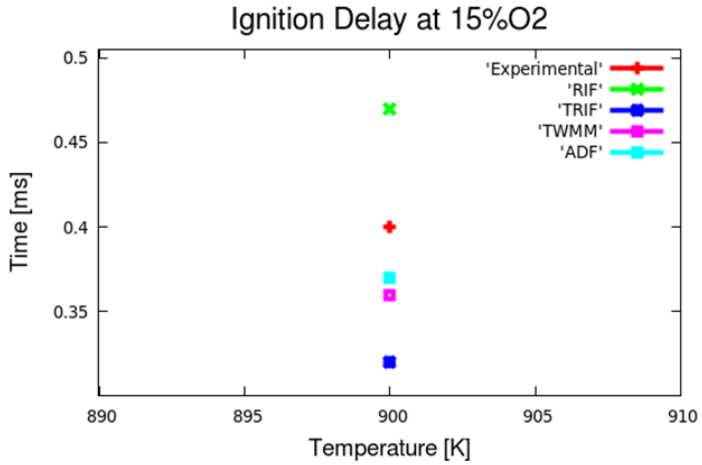

Figure 5.19: Ignition delay of RIF, TRIF, TWM and ADF models at 900K and 15%O_2 ambient condition

In Fig 5.20, 5.21, 5.22 and 5.23, spatial temperature distribution of Spray-A case is given for all combustion models with respect to 900 K and 15%O_2 ambient condition.

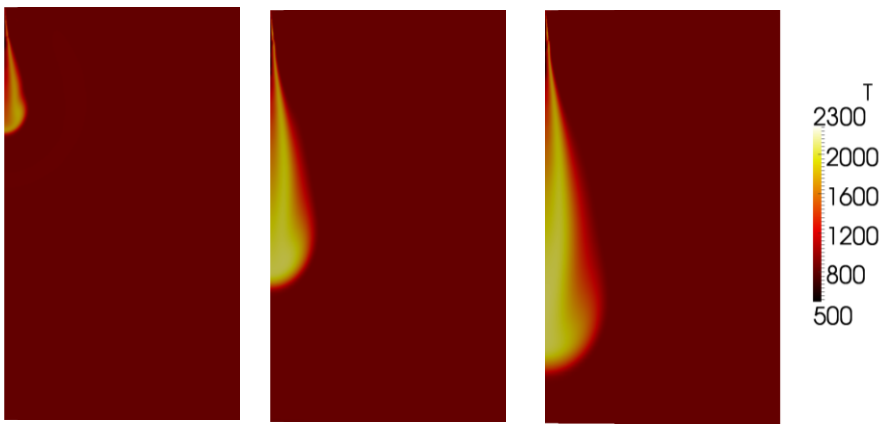

(a) 0.5 ms (b) 2 ms (c) 3.5 ms

Figure 5.20: Temperature spatial distribution with RIF model at 900K and 15%O_2 ambient condition

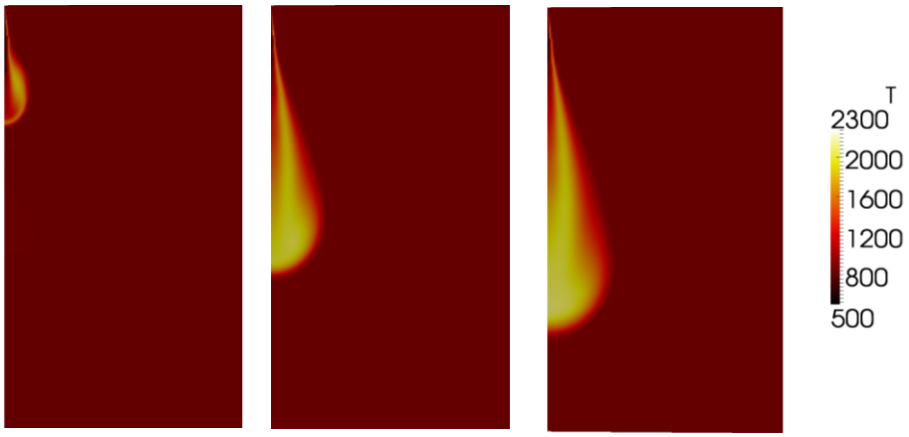

(a) 0.5 ms (b) 2 ms (c) 3.5 ms

Figure 5.21: Temperature spatial distribution with TRIF model at 900K and 15%O_2 ambient condition

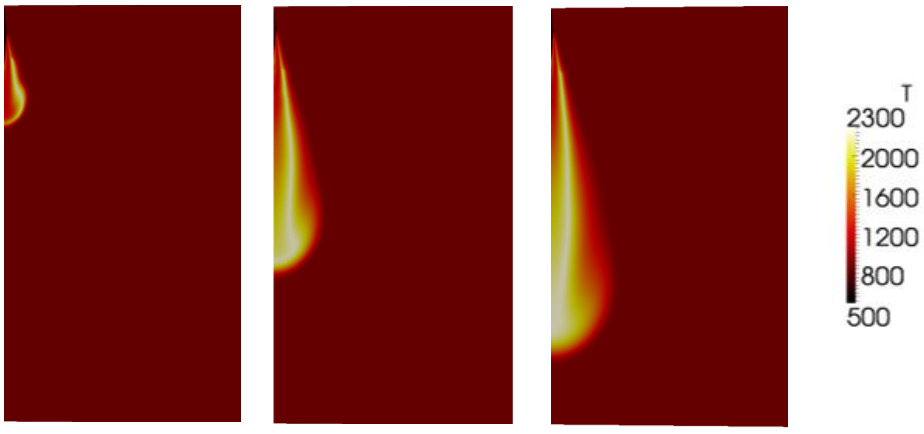

(a) 0.5 ms (b) 2 ms (c) 3.5 ms

Figure 5.22: Temperature spatial distribution with TWM model at 900K and 15%O_2 ambient condition

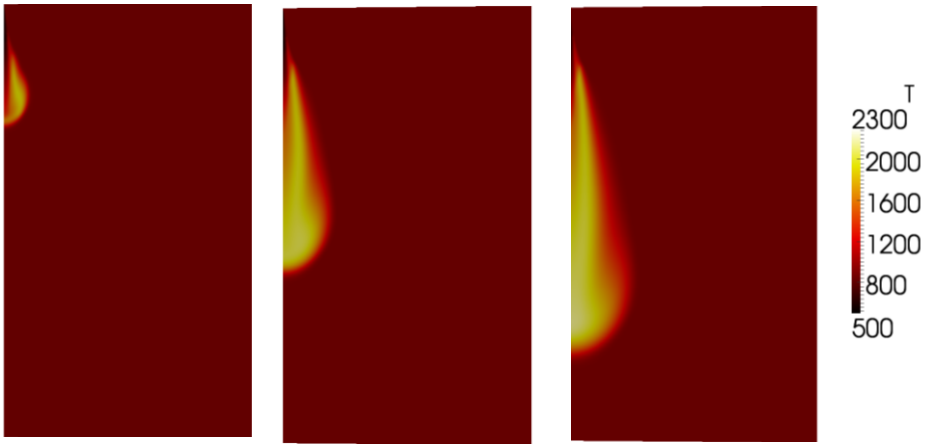

(a) 0.5 ms (b) 2 ms (c) 3.5 ms

Figure 5.23: Temperature spatial distribution with ADF model at 900K and 15%O_2 ambient condition

5.1.3 Soot Estimation

In this section soot results are discussed with respect to experimental data by using Tabulated Well-Mixed Model which is validated in section 5.1.2. Modeling approach for soot prediction is specified in section 4.1.2.5.

***alphaTa* [K]**	21100
***TaOx* [K]**	19680
***bBeta* [$\sqrt{m}/s$]**	6000
***cBeta* [-]**	9
***aAlpha* [1/s]**	10000
***etaColl* [-]**	0.13
***cOmegaOH* [kg.m/mol.s.$\sqrt{K}$]**	1
***cOmegaO2* [m/s]**	1
***Cmin* [-]**	100
***ScSoot* [-]**	0.75

Table 5.6: Soot model constants

Soot prediction is one of the most challenging topic of combustion modeling since it requires complex model which causes excessive process time. Consequently, some simplifications have to be done in order to reduce computational effort in order to apply the model for industrial application. This explains the reason for usage of TWM model in soot prediction process due to its simplification on turbulence-chemistry interaction in addition to tabulation of chemistry. To deal with soot, semi-empirical Leung Lundstedt Jones soot model is imposed into combustion model. The optimum constants for soot model are reported in Tab. 5.6.

The effects which have impact on the soot formation are lift-off length, ignition delay and oxidizing species.

While Lift-off Length (LOL) affects the position of soot clouds where higher lift-off value results higher soot clouds at downstream, ignition delay affects the position of soot clouds where lower ignition delay means lower distance of soot clouds to the injector. In addition to that, soot formation is affected by oxidizing species' quantity and position.

The main purpose of this section is to understand the behavior of soot formation under different operating conditions and try to obtain reliable outcomes in terms of trend of the results instead of exact values.

Soot analyses are conducted only at 900K condition with different oxygen concentration. While computational model is capable of estimation of soot mass under 15% oxygen condition, it is not able to estimate the trend correctly in other conditions. Fig. 5.24 shows the results obtained at 15% oxygen condition with respect to experimental data.

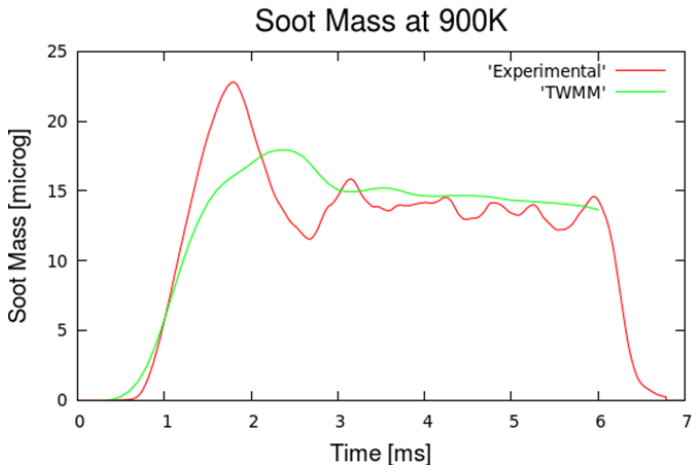

Figure 5.24: Integral soot mass results of TWM model and experiment at 900K and 15%O_2 ambient condition

As can be seen in the Fig. 5.24, soot formation is started earlier with respect to experimental data and the first peak is also delayed in TWM model. In addition to this, the value of the peak point is underestimated by TWM model. However, sufficient results are obtained in terms of total soot mas by combustion model (Only reliable for 15% oxygen concentration).

In Fig. 5.25 and 5.26, experimental and computational results for soot mass are given respectively for different oxygen concentration conditions.

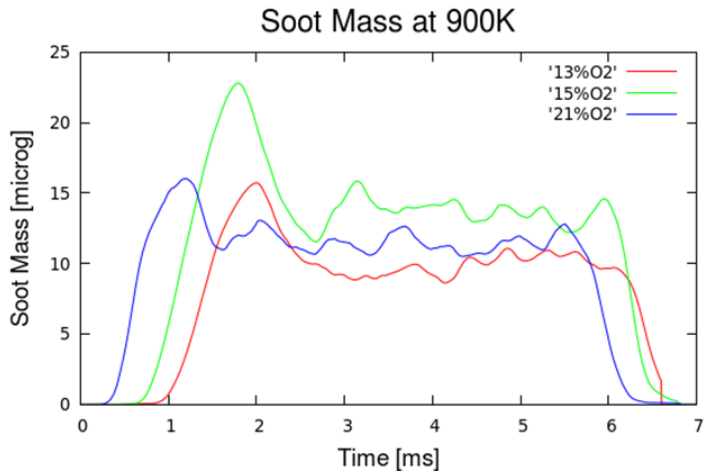

Figure 5.25: Experimental soot mass results at 900K ambient conditions

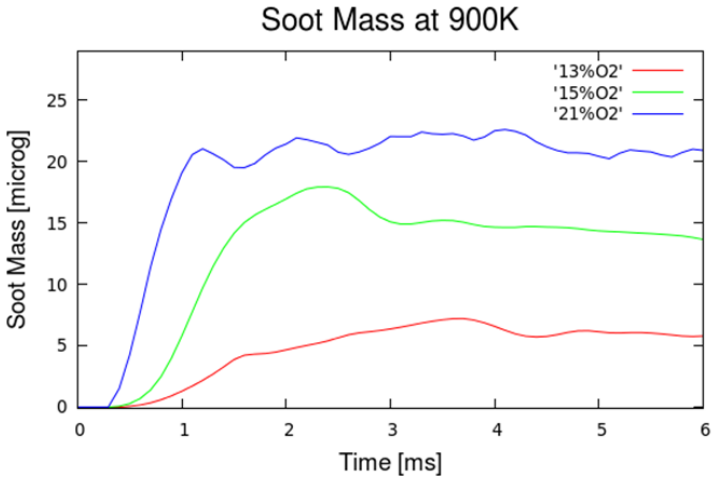

Figure 5.26: TWM model soot mass results at 900K ambient conditions

The soot model is not able to estimate the soot formation correctly in terms of maximum value, starting point and overall integral mass value at different operating situations. The behavior of the soot is explained with regards to experimental output. Start of soot formation value is the earliest for 21% oxygen condition and the latest for 13% oxygen condition. This trend can be simply explained by ignition delay. Lower ignition delay means lower the time for start of soot formation. Besides, the total soot mass is a compromise between lift-off length and availability of oxygen.

After obtaining the first soot results, a tuning process is applied to estimate the soot formation trend correctly. To achieve this, two parameters which are *cOmegaO2* and *cOmegaOH* are changed separately. The procedure is summarized in Tab. 5.7. Although some modifications are performed to obtain better results, sufficient results still cannot be reached by soot model with TWM model.

Tuning Number	**cOmegaOH**	**cOmegaO2**
1	0	0
2	55	0
3	106	0
4	0	1e2
5	0	1e4

Table 5.7: Tuning parameters for correct soot prediction process

5.2 DME Results

All combustion models are validated with Spray-A case and it can be stated that, models are able to predict fundamental feature of combustion process such as ignition delay, heat release rate and maximum temperature in vessel. Hence, in this section, DME fuel is analyzed with RIF model which is one of the already validated combustion models.

Initially simulations are performed with respect to condition defined in section 4.2.2. in order to investigate model behavior with different type of fuel other than conventional one. Then, ignition delay results are compared with the experimental data provided by [38, 39]. Finally, DME fuel is analyzed under

Spray-A operating conditions and a comparison is made between n-dodecane and dimethyl ether fuel.

First condition for DME is 40 MPa injection pressure, 1.7 MPa ambient pressure and 1084/980 K operating conditions. Accurate results are provided by RIF combustion model in terms of ignition delay with respect to experimental data [39] for the ambient conditions specified above. The ignition delay is represented in Fig. 5.27 and the values are specified in Tab. 5.8

	980 K	**1084 K**
RIF	2.1	1.2
Experimental	2.2	1.6

Table 5.8: Ignition delay values [ms] of RIF and experimental results for DME case at 40 MPa injection pressure

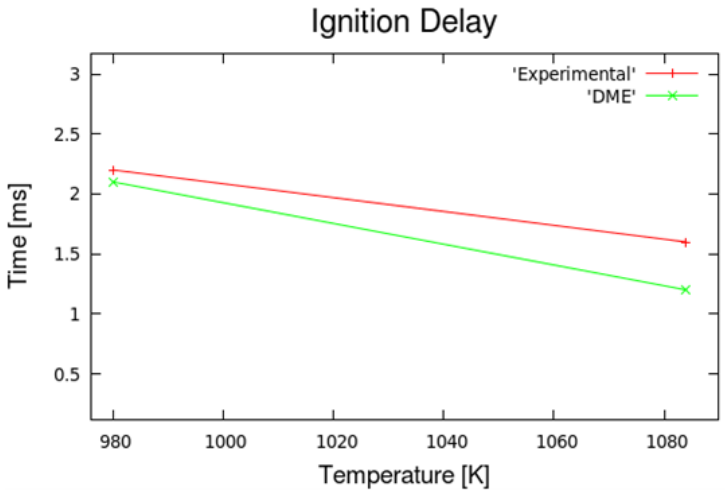

Figure 5.27: Ignition delay comparison of RIF with respect to experimental results for DME case at 40 MPa injection pressure

Another simulation is executed under 50 MPa injection pressure with 873 K and 7.04 MPa ambient condition. In this case, n-dodecane and DME fuels are analyzed together at same operating condition; however, injected fuel mass times

LHV of the fuels are not the same for both cases in this condition since injection pressure is kept constant for both models. Ignition delay values are reported in Tab. 5.9 and it represents a precise estimation with respect to results specified in the article [38].

	873 K
DME	0.55
n-dodecane	0.37

Table 5.9: Ignition delay values [ms] of DME and n-dodecane fuels with RIF model at 50 MPa injection pressure

As a final step, DME case is performed under Spray-A baseline ambient conditions; nevertheless, a modification on injection pressure is done. Injection pressure of the n-dodecane fuel is regulated as 10 MPa and dimethyl ether fuel is regulated to keep same amount of energy supply. Thus, injection pressure of dimethyl ether fuel is set as 17.5 MPa which is the value corresponding same amount of injected fuel mass times LHV of the fuel with n-dodecane case with 10 MPa injection pressure.

Fig. 5.28 and 5.29 illustrate the rate of heat release and maximum temperature behavior of different fuels respectively. As seen from the figure, n-dodecane has higher maximum value of the heat release rate. While DME fuel reaches the steady-state value of ROHR right after the auto-ignition phase, n-dodecane fuel reaches that value near the end of injection time which is 6 milli seconds. After the end of injection, n-dodecane case finishes the combustion process near the 7 milli seconds; however, combustion process of dimethyl ether still continues at 10 milli seconds. In addition to this, maximum temperature is reached faster by dimethyl ether fuel and n-dodecane reaches the maximum temperature value when the temperature of dimethyl ether starts to decrease.

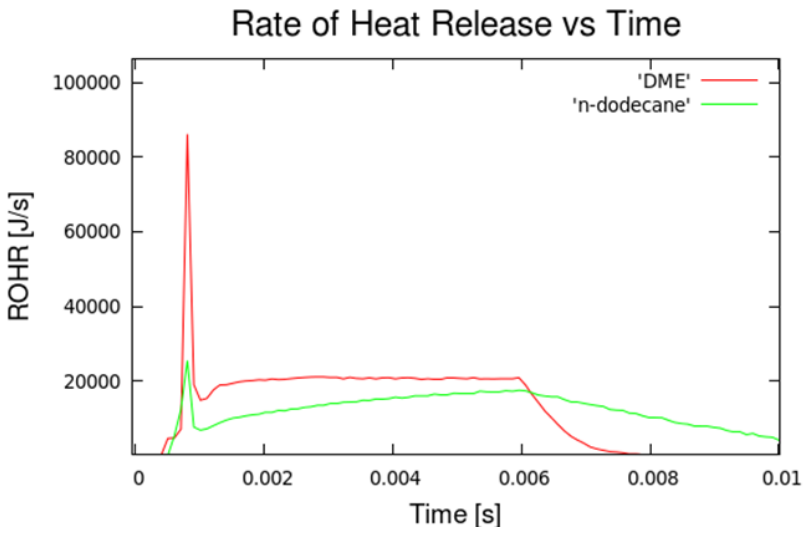

Figure 5.28: ROHR comparison of DME and n-dodecane fuel at 900K and 15%O_2 ambient condition with RIF model

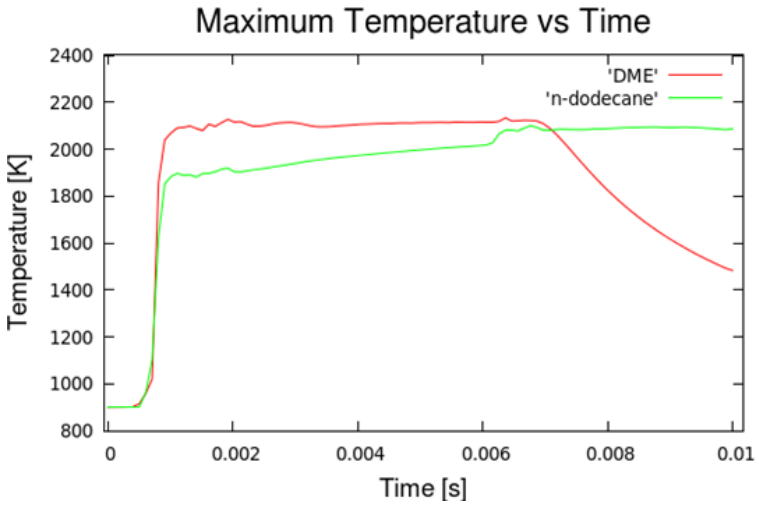

Figure 5.29: Maximum temperature comparison of DME and n-dodecane fuel at 900K and 15%O2 condition with RIF model

Ignition delays of n-dodecane and dimethyl ether fuels at 900 K and 15 %O_2 ambient conditions are shown (Fig. 5.30).

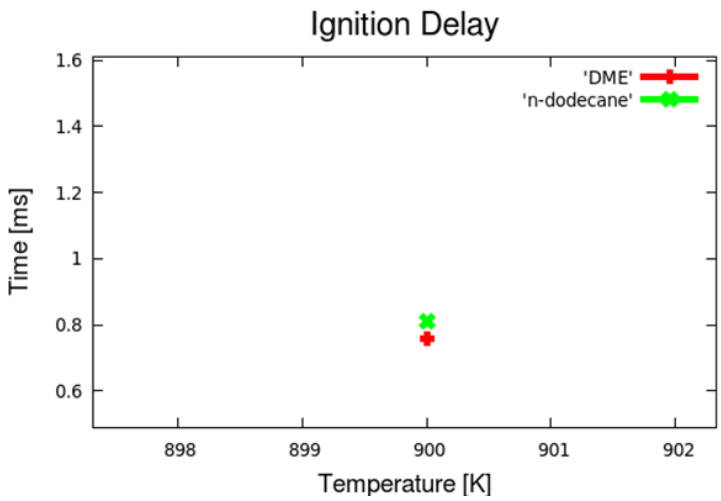

Figure 5.30: Ignition delay of DME and n-dodecane with RIF model at 900K and 15%O_2 ambient condition

To sum up, RIF model is able to predict DME fuel combustion process in terms of ignition delay. When DME and n-dodecane fuel has equal injection pressure, DME fuel ignites later than n-dodecane. However, if the total energy, obtained as fuel mass times LHV, supplied by fuels are constant, n-dodecane spray has a higher ignition delay compared to DME. In addition to that, it can be said that ignition delay has a decreasing trend for both fuels while ambient temperature increases.

Chapter 6

Conclusion

In this thesis, computational fluid dynamic analysis, where simulations are performed with open source OpenFOAM CFD software by adapting Lib-ICE which is developed by Politecnico di Milano Internal Engines Group, of the diesel combustion process is studied. Main purpose of the thesis is to investigate different combustion models, characterize their behavior and validate their accuracy under different operating conditions.

Initially, the theory of non-premixed combustion and modelling techniques for diesel combustion is discussed within the thesis and then combustion models which are used during this study are specified and explained. Furthermore, simulation setup, where injection profile, mesh, initial conditions and other parameters are set, is accomplished with respect to conditions which are provided by Sandia Laboratories. Simulations are performed under constant volume vessel due to accessibility of many experimental data.

In addition to validation of different chemical mechanisms and fuels with RIF Model, different combustion models which are RIF, TRIF, TWM and ADF are compared to each other by validating with experimental results. Main results obtained by chemistry validation are listed below:

- Both chemical mechanisms are able to produce accurate and similar results in terms of pressure rise, vapor penetration, heat release rate and maximum temperature.

- Although both chemical mechanisms do not correctly estimate the maximum value of heat release rate, YaoNC12 chemical mechanism is more capable to catch maximum point.

- Both chemical mechanisms give sufficient results in terms of ignition delay; however, YaoNC12 is able to estimate ignition delay value more accurate compared to NewAachenNC12 in general.

Moreover, combustion model comparison is performed after chemistry validation is obtained. Results from the analyses are listed as:

- All combustion models are successful to produce auto-ignition phase of the combustion process in terms of heat release rate at baseline condition. Transition time from auto-ignition region to diffusive combustion region is extended as TWM, RIF, ADF and TRIF where TWM model has the lowest value of time and TRIF model has the higher value of time.

- TRIF model gives the worst results except 1000K condition in terms of ignition delay where value of ID always is underestimated by TRIF and it is more sensitive to temperature compared RIF and TWM models. TRIF model always underestimates the value of maximum heat release value and the location of the maximum value under 15% oxygen conditions.

- Comparison of RIF and TWM models are performed in all conditions specified in this thesis. Both models reproduce accurate and similar results in terms of pressure rise and vapor penetration with respect to time. Maximum temperature within the vessel reaches a higher value for TWM model due higher burning rate. Both models are capable of reproducing the heat release curve in any conditions with small acceptable deviation. Even Though TWM model is able to obtain more accurate results compared to RIF model in terms of ignition delay, it is not able to give sufficient results for ignition delay trend under different oxygen content conditions particularly in the range of 15% and 21%.

- While required computational time for TWM model is half of the RIF model, it is slightly higher for TRIF and ADF models compared to TWM one.

Furthermore, soot formation estimation with TWM model is performed as a next step of this work. The outcomes for soot formation are:

- Model is able to result in terms of integral soot mass under 900K 15% oxygen condition. However, the start time of soot formation and the location of peak value of soot mass is not correctly estimated. In addition

to that, the model suffers from predicting soot trend under different oxygen levels.

- Some modifications are performed in order to match the soot rend of TWM model with experimental results; nevertheless, sufficient result cannot be obtained.

Finally, DME fuel as an alternative to conventional n-dodecane fuel for diesel engines is analyzed under different conditions:

- DME fuel is analyzed with RIF Model in particular condition in terms of ignition delay, and model is capable of predicting ignition delay with a good accuracy.

- A comparison between DME and n-dodecane fuel is achieved. While n-dodecane fuel has a shorter ignition delay at condition where injection pressure is constant for both fuels, DM fuel ignites faster at same amount of energy content condition.

Suggestion for further development of this research area are:

- Testing of ADF model under different operating condition to understand sensitivity of the model correctly.

- Analyzing the soot formation procedure in more detailed and extensive way and modification of the soot model in order to provide reliable results with respect to real condition.

- Extending the DME simulations by adapting different combustion models and different operating conditions.

Bibliography

[1] G. Ferrari, *Internal combustion engines*, Esculapio (2011).

[2] G. Ferrari, *Motori a combustione interna*, Il Capitello (1996).

[3] T. Poinsot, *Theoretical and numerical combustion*, Edwards (2012).

[4] G. Stiech, *Modeling engine spray and combustion process,* Springer (2003).

[5] J. B. Heywood, *Internal combustion engine fundamentals,* McGraw-Hill (1988).

[6] H.K. Versteeg, W. Malalaskera, *An introduction to computational fluid dynamics the finite volume methods,* Longman (1995).

[7] S. B. Pobe, *Computationally efficient implementation of combustion chemistry using in situ adaptive tabulation,* Combustion Theory Modeling 1, 41-63 (1997).

[8] G. D'Errico, T. Lucchini, F. Contino, M. Jangi, X. S. Bai, *Comparison of well-mixed and multiple representative interactive flamelet approaches for diesel spray combustion modelling,* Combustion Theory and Modelling, 18:1, 66-88 (2014).

[9] G. D'Errico, D. Ettore, T. Lucchini, *Simplified and detailed chemistry modeling of constant-volume diesel combustion experiments,* SAE International, 2008-01-0954 (2008).

[10] Z. Ren, G. M. Goldin, V. Hiremath, S. B. Pobe, *Reduced description of reactive flows with tabulation of chemistry,* Combustion Theory and Modelling, 15:6, 827-848 (2011).

[11] F. Contino, J. Masurier, F. Foucher, T. Luchhini, G. D'Errico, P. Dagaut, *CFD simulations using the TDAC method to model iso-octane combustion for a large range of ozone seeding and temperature conditions in a single cylinder HCCI engine,* Fuel 137, 179-184 (2014).

[12] M. A. Singer, S. B. Pobe, *Exploiting ISAT to solve the reaction-diffusion equation,* Combustion theory and modelling, 8:2, 361-383 (204).

[13] B. Franzelli, B. Fiorina, N. Darabiha, *A tabulated chemistry method for spray combustion,* Proceedings of the combustion institute 34, 1659-1666 (2012).

[14] H. Wang, Y. Chen, *PDF modelling of turbulent non-premixed combustion with detailed chemistry,* Chemical engineering science 59, 3477-3490 (2004).

[15] G. Lacaze, J. C. Oefelein, *A non-premixed combustion model based on flame structure analysis at supercritical pressures,* Combustion and Flame 159, 2087-2103 (2012).

[16] G. D'Errico, T. Luchhini, G. Hardy, F. Tap, G. Ramaekers, *Combustion modeling in heavy duty diesel engines using detailed chemistry and turbulence-chemistry interaction,* 2015-01-0375 (2015).

[17] C. Hasse, H. Barths, N. Peters, *Modelling the effect of split injections in diesel engines using representative interactive flamelets,* SAE technical paper, 1999-01-3547 (1999).

[18] G. D'Errico, D. Ettore, T. Lucchini, *Comparison of combustion and pollutant emission models for DI diesel engines,* SAE technical paper, 2007-24-0045 (2007).

[19] https://ecn.sandia.gov/diesel-spray-combustion/sandia-cv/.

[20] https://ecn.sandia.gov/ecn-data-search/.

[21] https://ecn.sandia.gov/diesel-spray-combustion/target-condition/.

[22] T. Yao, Y. Pei, B. Zhong, S. Som, T. Lu, *A hybrid mechanism for n-dodecane combustion with optimized low-temperature chemistry,* 9th U.S. National combustion meeting (2015).

[23] T. Lucchini, G. D'Errico, A. Onorati, A. Frassoldati, A. Stagni, *Modeling non-premixed combustion using tabulated kinetics and different flame structure,* SAE Int. J. Engines 10(2): 2017 (2017).

[24] T. Lucchini, G. D'Errico, T. Cerri, A. Onorati, G. Hardy, *Experimental validation of combustion models for diesel engines based on tabulated kinetics in a wide range of operating conditions,* SAE technical paper 2017-24-0029 (2017).

[25] F. Contino, H. Jeanmart, T. Luchhini, G. D'Errico, *Coupling of in situ adaptive tabulation and dynamic adaptive chemistry: An effective method*

for solving combustion in engine simulations, Proceedings of the Combustion Institute 33, 3057-3064 (2011).

[26] *OpenFOAM user guide version 4.0*, OpenFOAM Foundation (2016).

[27] *Worldwide emission standards and related regulations,* Continental (2017).

[28] K. Lindqvist, *Emission standards for light and heavy road vehicles,* AirClim (2012).

[29] A. Frassoldati, G. D'Errico, T. Luchhini, A. Stagni, A. Cuoci, T. Faravelli, A. Onorati, E. Ranzi, *Reduced kinetic mechanism of diesel fuel surrogate for engine CFD simulations,* Combustion and flame 162, 3991-4007 (2015).

[30] G. Derrico, T. Lucchini, A. Onorati, G. Hardly, *CFD modelling of combustion in heavy-duty diesel engines,* THIESEL (2014).

[31] R. D. Reitz, *Modeling atomization process in high pressure vaporizing sprays,* Atomization and spray technologies 3, 309-337 (1987).

[32] *A technical summary of Euro 6/VI vehicle emission standards,* The international council of clean transportation (2016).

[33] T. Lucchini, *Lib-ice: code structure and capabilities,* Politecnico di Milano.

[34] R. Aglave, U. Riedel, J. Warnatz, *Turbulence-chemistry interactions in CFD modelling of diesel engines,* Combustion theory and modelling, 12:2, 305-325 (2008).

[35] H. Guo, F. Liu, G. Smallwood, *Soot and NO formation in counterflow ethylene/ oxygen/ nitrogen diffusion flames,* 8:3, 475-489 (2004).

[36] K. M. Leung, R. P. Lindstedt, W. P. Jones, *A simplified reaction mechanism for soot formation in non-premixed flames,* Combustion and flame 87, 289-305 (1991).

[37] L. Cai, L. Kroger, H. pitsch, *Reduced and optimized mechanism for n-Dodecane oxidation,* 15th International conference on numerical combustion.

[38] S. Lee, Y. Murata, Y. Dalsho, *Spray and combustion characteristics of dimethyl ether fuel,* Proceedings of the institution of mechanical engineers part d journal of automobile engineers 219(1), 97-102 (2015).

[39] Y. Kim, J. Lim, K. Min, *A study of the dimethyl ether spray characteristics and ignition delay,* International journal of engine research 8(4), 337-346 (2007).

[40] M. Yao, Z. Zheng, S. Xu, M. Fu, *Experimental study on the combustion process of dimethyl ether (DME),* SAE technical paper, 2003-01-3194 (2003).

[41] A. Bhagatwala, T. Lu, H. Shen, J. A. Sutton, J. H. Chen, *Numerical and experimental investigation of turbulent DME jet flames,* Proceedings of the combustion institute 35(2), 1157-1166 (2014).

[42] N. Peters, *Laminar flamelet concepts in turbulent combustion,* 21st Sypmosium (International) on combustion, 1231-1250 (1986).

[43] N. Peters, *Laminar diffusion flamelet models in non-premixed turbulent combustion,* Prog energy combust Sci 10, 319-339 (1984).

[44] F. Payri, R. Novella, J.M. Pastor, E.J. Perez-Sanchez, *Evaluation of the approximated diffusion flamelet concept using fuels with different chemical complexity,* Applied mathematical modelling 49, 354-374 (2017).

[45] J.M. Desantes, J.M. Garcia-Oliver, R. Novella, E.J. Perez-Sanchez, *Application of an unsteady flamelet model in a RANS framework for spray A simulation,* Applied thermal engineering 117, 50-64 (2017).

[46] https://www.cmt.upv.es/ECN03.aspx/.